A MOC-based neutron kinetics model for noise analysis

A MOC-BASED NEUTRON KINETICS MODEL FOR NOISE ANALYSIS

Gammicchia A.[a], **Santandrea S.**[a], **Zmijarevic I.**[a], **Sanchez R.**[a], **Stankovski Z.**[a], **Dulla S.**[b], **Mosca P.**[a]

[a] *DEN-Service d'études des réacteurs et de mathématiques appliquées (SERMA)*
CEA, Université Paris-Saclay, F-91191, Gif-sur-Yvette, France
[b] *Politecnico di Torino, Dipartimento Energia, NEMO Group*
Corso Duca degli Abruzzi 24, 10129 Torino, Italy

Abstract

A 2-D noise model is implemented in the deterministic reactor code APOLLO3® to simulate a periodic oscillation of a structural component. The Two/Three Dimensional Transport (TDT) solver, using the Method of Characteristics, is adopted for the calculation of the case studies, constituted by a moving detector and control-rod bundle. The periodic movement is built by properly linking the geometries corresponding to the temporal positions. The calculation is entirely performed in the real time domain, without resorting to the traditional frequency approach. A specifically defined *dynamic eigenvalue* is used to renormalize in average the reactivity over a period. The algorithm is accelerated by the DP_N synthetic method. For each cell of the domain, the time values of fission rates are analysed to determine the noise extent. Moreover we propose a systematic approach to the definition of the macroscopic cross sections to be used in dynamical calculations starting from library data. As an aside of our work we have found that even in static calculation this approach can produce significant changes.

Keywords: Neutron noise, Neutron kinetics, 2D MOC

1. INTRODUCTION

Neutron noise theory has its origins in the experiments performed at the "Clinton Pile" of Oak Ridge in the 1940s (Pázsit and Demazière, 2010), whose goal was the evaluation of absorption cross sections of various elements. Although they did not concern diagnostics at all, these experiments contemplated, for the first time, neutron oscillations. The analyses of these measurements were collected in a paper by Weinberg and Schweinler (1948).

In reactor physics the so-called "power reactor noise" (Pázsit and Demazière, 2010) is the effect on the neutron flux of the oscillatory perturbation of macroscopic cross sections, due either to vibrations of the structural components or to fluctuations of the coolant density. Whenever these excursions exceed the safety limits, the noise signal can be analysed to identify and localize malfunctions without the need of intrusive

Email addresses: andrea.gammicchia@cea.fr (**Gammicchia A.**), simone.santandrea@cea.fr (**Santandrea S.**), igor.zmijarevic@cea.fr (**Zmijarevic I.**), richard.sanchez@cea.fr (**Sanchez R.**), zarko.stankovski@cea.fr (**Stankovski Z.**), sandra.dulla@polito.it (**Dulla S.**), pietro.mosca@cea.fr (**Mosca P.**)

diagnostics, hence there is a strong interest in improving the detection and the analysis of this signal.

Traditionally, neutron noise can be simulated by a stochastic model generating the small deviations randomly or by considering a given, periodic modification of cross sections (Sanchez, 2015). In both cases the starting point is a critical condition and the cross-section variation, acting as noise source, produces fluctuations in the neutron flux which can be either random or deterministic, depending on the nature of the source (Pázsit and Demazière, 2010). The classical way to study oscillations of nuclear properties adopts a frequency-based approach: a system of linearized equations in the frequency domain, derived from the linear transport equation through Fourier transform, is solved to obtain the coefficients needed to reconstruct the flux temporal behavior. A drawback of this procedure is the appearance of a frequency dependence in the cross sections, with consequent complications in the numerical discretizations. Moreover, this approach is based on the assumption that properties undergo small variations. So even if the standard approach deserves attention, we believe that there is a true interest in developping a non-perturbative methodology that does not need complex-valued cross sections, and which can share most of its discretization hypotheses with standard temporal-based kinetics schemes, as the one discussed in the present paper.

A deterministic method is here presented, aiming to simulate the periodic oscillation of a system component. The period is discretized into a set of sub-intervals, and each of them is associated to a geometric configuration, that is, to a position of the component. In doing so, noise is studied within the real temporal domain, without the need of the "small-perturbation assumption". In fact, starting from a critical, unperturbed condition, any deviation from the average criticality is taken into account by a "dynamic eigenvalue" defined ad hoc. The computational scheme is realized inside the TDT (Two/Three Dimensional Transport) solver (Santandrea, 2007; Santandrea et al., 2017) and implemented in the APOLLO3® system. Another example, still based on temporal discretization, is given in Viebach et al. (2018): in the framework of the DYN3D code, noise calculations are performed in the time domain and within a fully multi-physics framework, including the system feedback to establish criticality during the noise perturbation. The main difference of our approach, with respect to DYN3D one, is the fact that we do not make a full *analogical* calculation of the dynamics preceding the regular oscillatory final state. In our approach we directly compute this final oscillatory state with a new equation conceived to represent the harmonic response of the system.

The paper describes first the physical aspects of the problem, the equations involved as well as their specialization to the case in question; this is done in Section 2. Section 3 presents a systematic procedure to *translate* the isotopic nuclear data that can be found in external libraries, into the *per delayed family* macroscopic form that is used in habitual Kinetic equations. In our opinion this stage is usually performed in heuristic way, while we are proposing a rigorous way of retrieving these macroscopic data from their microscopic counterparts. Section 4 deals with the resolution strategy, which is basically an adaptation of the classical power method, and its acceleration is described in Section 5. In Section 6 the characteristics of the considered geometries are addressed, showing the component displacements and the obtained results in terms of dynamic eigenvalues and fission-rate oscillation amplitude. Lastly, Section 7 reports conclusions

and future perspectives of the presented noise approach.

2. THE NEUTRON KINETIC PROBLEM REVISITED FOR NOISE

The neutron transport kinetic problem (Keepin, 1965) can be classically written as a set of integro-differential equations, the first part of which governs the evolution of the so-called family of delayed-neutron precursors, with the last one being the neutron flux kinetic equation. As for per-family precursor concentrations, the equations are:

$$\partial_t C_i(\vec{r},t) = -\lambda_i C_i(\vec{r},t) + \bar{\beta}_i(\vec{r},t)\int_E dE'(\nu\Sigma_f\phi)(\vec{r},E',t), for\ i = 1, N_{delayed}, \tag{1}$$

while the neutron flux obeys:

$$\left(\frac{1}{v}\partial_t + \mathcal{L}\right)\psi(\vec{r},\vec{\Omega},E,t) - \mathcal{H}\psi(\vec{r},\vec{\Omega}',E',t) = q(\vec{r},\Omega,\vec{E},t) +$$
$$\sum_{j=1}^{N_f}\sum_{M=1}^{MG}\bar{\chi}^p_{j,M}(\vec{r},E,t)\int_{E_M} dE'\left(1-\beta^j(E')\right)(\nu\Sigma_{f,j}\phi)(\vec{r},E',t) +$$
$$\sum_{i=1}^{N_{delayed}}\bar{\chi}^d_i(\vec{r},E,t)\lambda_i C_i(\vec{r},t) = q + \mathcal{F}_p\phi + \mathcal{F}_d\vec{C}, \tag{2}$$

and these equations constitute a closed system. In the last line we have implicitly defined *prompt* and *delayed* fission operators and we have added a supplementary external source q. The rest of notations is described next:

$\mathcal{L}$**:** the transport operator (streaming and total collision).

$\mathcal{H}$**:** the transfer operator.

$\psi(\vec{r},\vec{\Omega},E,t)$**:** the angular neutron flux at energy E and time t.

$\Sigma_{f,j}$**:** the macroscopic fission cross section for isotope j, that is to say $\Sigma_{f,j} = c_j * \sigma_{f,j}$ the product of the isotope concentration time the microscopic cross section.

$\Sigma_f(\vec{r},E',t)$**:** the total fission cross section, equal to $\sum_{j=1,N_f}\Sigma_{f,j}(\vec{r},E',t)$.

MG**:** the number of macro-groups on which the fission integral has been decomposed (Mosca et al., 2013), E_M is the energy interval of the M-th macro-group.

$N_f(\vec{r})$**:** the number of types of fissile isotopes at position $\vec{r}$, that appears in the definition of $\Sigma_f(\vec{r},E',t)$.

$\phi(\vec{r},E',t) = \int_{4\pi} d\vec{\Omega}\psi(\vec{r},\vec{\Omega},E',t)$**:** the scalar neutron flux.

$\bar{\chi}^p_{j,M}(\vec{r},E,t)$**:** the prompt energy spectrum of neutrons emitted by fission of the isotope j when the incident neutron impacts the atomic nucleus in the energy range E_M.

$N_{delayed}$**:** the number of families of delayed precursors.

$\bar{\chi}_i^d(\vec{r}, E, t)$**:** the energy spectrum of delayed emission due to the decay process of precursors of the i-th family at position $\vec{r}$.

$\bar{\beta}_i$**:** the fraction of delayed neutrons for the i-th family.

β^j**:** the fraction of delayed neutrons for the j-th isotope.

$C_i(\vec{r}, t)$**:** the delayed precursor concentration of the i-th family.

λ_i the decay constant of the i-th family of precursors.

We note explicitly that in our formulas (1) and (2) all kinetic parameters bear an *over bar* averaging operator that makes these functions spatial dependent. This non-classical feature is due to the way we deduce these macroscopic quantities from microscopic data and is explained in Sec. 3. In this respect it is interesting to note that while β^j is not averaged, the analogous quantity for the *family*, $\bar{\beta}_i(\vec{r}, t)$, is.

2.1. Delayed Fission Source Treatment

For consistency, from the assumption we have made about the periodic variation of cross sections, it follows that also the flux and the precursor concentrations have to be a T-periodic function. Therefore, the sum over fissile isotopes $\sum_j$ present in (2) is also T-periodic. In order to express the delayed contribution to the fission source in terms of the variable flux, the precursor equations are firstly integrated over time: thanks to periodicity this step leads to write for each family i

$$C_i(\vec{r}, t) = \int_0^T dt' \left(\frac{e^{-\lambda_i T}}{1 - e^{-\lambda_i T}} + \theta_{[0,t]}(t') \right) e^{-\lambda_i (t - t')} f_i(\vec{r}, t'), \tag{3}$$

where T is the period of the oscillation, $\theta_{[0,t]}(t')$ is the characteristic function of the time interval $[0, t]$, equal to 1 if $t' \in [0, t]$ and to 0 otherwise, and

$$f_i(\vec{r}, t') = \bar{\beta}_i(\vec{r}, t') \int_E dE' (\, \nu\Sigma_f \phi)(\vec{r}, E', t') \tag{4}$$

represents the fraction of precursors of the family i generated from fissions.[1]

This result is then substituted in the last term of the neutron kinetic equation, which, due to the time integral of Eq. (3), at each time t is now dependent on the flux behavior over the entire period. However, the constraints of the numerical discretization limit the number of available flux solutions to the number N of period sub-intervals. In order to write a numerical form for the precursor production term in Eq. (4), the time period is discretized in N uniform sub-intervals, each one identified by the index k and centered around the instant $t_k = (k - 1/2)\frac{T}{N}$. To approximate the time integral a quadrature formula is then developed,

[1] Eq. (3) can be readily obtained after expressing the initial-final precursor concentration from the following equation

$$C_i(\vec{r}, 0) = C_i(\vec{r}, T) = C_i(\vec{r}, 0) e^{-\lambda_i T} + \int_0^T dt' e^{-\lambda_i (T - t')} f_i(\vec{r}, t'),$$

for which the condition is imposed that it solves exactly the integral of any T-periodic function containing terms up to a certain frequency, based on the chosen number of sub-intervals. Therefore, the delayed source in the sub-interval centered around the instant t_k reads

$$\sum_i \bar{\chi}_i^d(\vec{r},E,t_k)\lambda_i C_i(\vec{r},t_k) = \sum_i \bar{\chi}_i^d(\vec{r},E,t_k)\lambda_i \sum_{k'=1}^{N} w_{i,k}(t_{k'}) f_i(\vec{r},t_{k'}), \tag{5}$$

$w_{i,k}(t_{k'})$ being the k'-th weighting coefficient for delayed family i at time t_k. This means that for each pair (i,t_k) a new set of weights has to be computed, corresponding to all kinetic families and all discretization points of the period.

2.2. Quadrature formula for the delayed source

We note that the assumed periodicity of the precursor concentration in Eq. (3) requires the periodicity of the precursor production term in Eq. (4) which in turn, because the perturbed cross sections are periodic, depends on the periodicity of the angular flux. In order to write a numerical form for the precursor production term we use the fact that the function $f_i(t')$ is periodic with period T and that therefore it can be expanded into a Fourier series over the set of functions, $\cos(\omega_n t)$ and $\sin(\omega_n t)$ with $\omega_n = (2\pi n)/T$ and $n \geq 0$.

Thus, taking into account the periodicity we want the quadrature weights in Eq. (5) to preserve the analytical value of the integral with any T-periodic function in place of the sum, up to a given order of approximation. This can be done up to a certain frequency, depending on the available time steps. The integrals we want to conserve are therefore the following:

$$\int_0^T dt' \left(\frac{e^{-\lambda_i T}}{1-e^{-\lambda_i T}} + \theta_{[0,t]}(t') \right) e^{-\lambda_i (t-t')} e^{i_u \omega_n t'}, \qquad n = 0,..,N/2, \tag{6}$$

where N is a given even number, and whose analytical values are

$$\frac{\lambda_i cos\big(\omega_n t\big) + \omega_n sin\big(\omega_n t\big)}{\lambda_i^2 + \omega_n^2} + i_u \frac{\lambda_i sin\big(\omega_n t\big) - \omega_n cos\big(\omega_n t\big)}{\lambda_i^2 + \omega_n^2}, \qquad n = 0,..,N/2. \tag{7}$$

i_u is the imaginary unit (where the u subscript is used to distinguish it from the index i) and n is an integer number determining the frequency n/T of the periodic function that appears in the integral so that $\omega_n = (2\pi n)/T$. Since $\exp(i_u \omega_n t') = \cos(\omega_n t') + i_u \sin(\omega_n t')$, it follows that the real part of (7) is due to the contribution of $\cos(\omega_n t')$, while the imaginary part arises from the $\sin(\omega_n t')$. For this reason, and to obtain a unique solution for the weighting coefficients, an equation for sines and one for cosines are to be considered for each value of n except for 0 and $N/2$; for the latter we have decided to write a sine equation, whereas the former leads to an equation with unit coefficients. For each pair (i,t_k) the number of equations for weights is equal to that of time steps. Now we can use these equations requiring that $\int_0^T dt' \left(\frac{e^{-\lambda_i T}}{1-e^{-\lambda_i T}} + \theta_{[0,t_k]}(t') \right) e^{-\lambda_i (t_k - t')} f_i(t') \approx \sum_{k'=1}^{N} w_{i,k}^{k'} f_i(t_{k'})$, where the unknown vector $\vec{w}_{i,k}$ of weights is obtained under the condition of reproducing the analytic integral of Eq. (6). A system of the form $\mathcal{A}\vec{w}_{i,k} = \vec{b}_{i,k}$ has then to be solved, where $\vec{w}_{i,k}$ is the unknown vector of the N weights for the pair (i,t_k),

and matrix $\mathcal{A}$ is constructed as

$$\mathcal{A} = \begin{bmatrix} 1 & 1 & 1 & \dots & 1 \\ \sin(\omega_1 t_1) & \sin(\omega_1 t_2) & \sin(\omega_1 t_3) & \dots & \sin(\omega_1 t_N) \\ \cos(\omega_1 t_1) & \cos(\omega_2 t_2) & \cos(\omega_2 t_3) & \dots & \cos(\omega_2 t_N) \\ \sin(\omega_2 t_1) & \sin(\omega_2 t_2) & \sin(\omega_2 t_3) & \dots & \sin(\omega_2 t_N) \\ \vdots & \vdots & \vdots & \ddots & \vdots \\ \sin(\omega_{N/2} t_1) & \sin(\omega_{N/2} t_2) & \sin(\omega_{N/2} t_3) & \dots & \sin(\omega_{N/2} t_N) \end{bmatrix}$$

and $\vec{b}_{i,k}$ contains the analytic values of the integrals, arranged as follows:

$$\vec{b}_{i,k} = \begin{bmatrix} \frac{1}{\lambda_i} \\ \frac{\lambda_i \sin(\omega_1 t_k) - \omega_1 \cos(\omega_1 t_k)}{\lambda_i^2 + \omega_1^2} \\ \frac{\lambda_i \cos(\omega_1 t_k) + \omega_1 \sin(\omega_1 t_k)}{\lambda_i^2 + \omega_1^2} \\ \frac{\lambda_i \sin(\omega_2 t_k) - \omega_2 \cos(\omega_2 t_k)}{\lambda_i^2 + \omega_2^2} \\ \vdots \\ \frac{\lambda_i \sin(\omega_{N/2} t_k) - \omega_{N/2} \cos(\omega_{N/2} t_k)}{\lambda_i^2 + \omega_{N/2}^2} \end{bmatrix}.$$

We remind the reader that computing the weights in this way is equivalent to saying that, if our periodic function were equal to $\sum_{n=1}^{N/2-1}\left[c_{2,n}cos\left(\omega_n t\right)+c_{1,n}sin\left(\omega_n t\right)\right]+c_{1,N/2}sin\left(\omega_{N/2}t\right)+c_{2,0}$, with $c_{1,n}$ and $c_{2,n}$ arbitrary constant values, our approximation would exactly reproduce the $C_i(t_k), k=1,N$ values of the delayed precursor concentrations for each family at each computational time as well as the initial $C_i(0)$ concentration. This shows that our technique is able to integrate exactly a trigonometric base of order N with N points. This means that we preserve $N*N*N_{delayed}$ integrals with the help of N points and $N*N*N_{delayed}$ weights. However, it is important to note that our computational cost is only proportional to N, which makes our formula very attracting, in our opinion. In a first phase of this work we have used the Gauss-Legendre quadrature formula to approximate the integral in (6). The issues of using formulas like the Gauss-Legendre one is that they do not grant the exact integration of the integrals involved into the $C_i(t_k), k=1,N$ quantities (when one supposes that the fission sources are, let say, polynomial) due to the decay exponential appearing inside it. Of course one could correct this by using quadrature formulas of the Gauss family with the positive exponential weight. But the set of families of quadrature formulas that *optimally* integrate different exponentials do not share the same points as our formula does. And this clearly makes their use less profitable than the quadrature we have chosen.

We end with a remark. As it is well known from discrete Fourier analysis, $\mathcal{A}$ owns an analytical inverse (Hildebrand, 1954), which is

$$\mathcal{A}^{-1}=\mathcal{G}\ Tr(\mathcal{A}), \tag{8}$$

where Tr stands for the transpose operator, while $\mathcal{G}$ is a diagonal matrix whose elements are $\mathcal{G}_{i,i}=\frac{1}{N}$ for $i\neq 1,N$ or $\mathcal{G}_{i,i}=\frac{2}{N}$ for $i=1,N$. This implies that the analytical form of the computed weights is

$$w_{i,k}(t_j)=\mathcal{G}_{i,i}\Big[\lambda_i+\sum_{l=1}^{N}\frac{\lambda_i\sin\left(\omega_l t_k\right)-\omega_l\cos\left(\omega_l t_k\right)}{\lambda_i^2+\omega_l^2}\sin\left(\omega_l t_j\right)+\frac{\lambda_i\cos\left(\omega_l t_k\right)+\omega_l\sin\left(\omega_l t_k\right)}{\lambda_i^2+\omega_l^2}\cos\left(\omega_l t_j\right)\Big]. \tag{9}$$

2.3. Time discretization

As we discuss in subsection 2.1, the time discretization is based on a constant time step $\Delta=T/N$ for N even. We shall compute the solution at the step-centered N times $t_k=(k-1/2)\Delta$, for $k=1,\cdots,N$. At each time step we solve the transport equation using the method of characteristics where the energy range is discretized into a set of groups, a discrete ordinates approximation is used for the angular direction and the geometry domain is partitioned into a set of homogeneous regions on which the angular moments of the flux are taken to be uniform. The angular directions come from an angular quadrature which is also used to compute the angular flux moments from the angular fluxes. The latter are iteratively computed from the region wise flat sources by sweeping the domain along a prescribed set of straight parallel trajectories for each of the angular directions (Santandrea et al., 2017).

In the kinetic noise problems that we have considered the geometrical domain consists of two parts: one where the material compositions do not change with time and a second part where they do. Therefore, we have adopted a Lagrangian approach whereupon the equations are described in a coordinate frame that moves with the local material velocity $\vec{u}(\vec{r},t)$. In the part of the geometry where the material remains constant in time, $\vec{u}=0$ and the reference frame is Eulerian. In contrast, in the domain with moving materials we write the neutron transport equation in a moving frame. This entails a major modification in that the Eulerian time derivative ∂_t has to be replaced by the Lagrangian material derivative $d_t=\partial_t+\vec{u}\cdot\nabla$. For convenience we have also used a Lagrangian spatial mesh to construct the regions at the different discretization times. The spatial mesh is defined for the material distribution at the steady-state equilibrium before the onset of the periodic vibrations and, for every time t_k, it is obtained by moving the mesh to its position at time t_k. For the simple case of a periodic motion with fixed direction this means that a solid material region D_i defines a similar material region $D_i(t_k)$ uniformly translated by the periodic vector $\vec{\epsilon}(t_k)$ that gives the displacement at time t_k from the steady-state position for any point of the moving solid regions. Clearly, a limitation of the periodic motion is that moving solid components cannot enter a non moving solid component. On the other hand, the regions occupied by the coolant comprised between moving and non moving solids will change of size and shape with time. See, for example, Fig. 3. A potential difficulty with the use of a Lagrangian reference frame is that in a moving frame the media become anisotropic and the cross sections depend then on the neutron direction. But, in noise analysis this effect is negligible because the maximum vibration speed is orders of magnitude smaller than the mean speed of the bulk of the thermal neutrons.[2]

An annoying effect of periodic material vibrations is that the vibration adds a nonzero amount of reactivity to the system. Consider, for instance a pin vibrating near fuel pins that remain at rest. During a period the vibrating pin will expend more time far from its equilibrium position than near to it. If the vibrating pin is also a fuel pin the result will be that an amount of positive reactivity will be added to the system every period, whereas for a vibrating absorbing pin the effect will be a negative amount of reactivity. The change in reactivity can be controlled by natural feedback mechanisms as well as, in power reactor, by artifical control means, so instead of getting out of equilibrium, the system might slightly change its power output and reach a close steady-state regime. Furthermore, it has also been shown that accounting for the feedback mechanisms in the noise simulation not only regularizes the noise equations but it also ensures the periodicity of the solution (Sanchez, 2015). In previous work this has been done by introducing a small scalar operator. This operator amounts to an anisotropic contribution to the total cross section and it is iteratively computed so as to set to zero the period averaged noise-induced reactivity (Sanchez, 2015; Rouchon, 2016). Instead, in the present work, where we deal with the full time-dependent noise equations, we have opted for introducing a dynamic eigenvalue k_D which, again, is iteratively calculated so as to ensure that the period-averaged

[2]For example, for the sinusoidal vibration considered in subsection 5.2 the maximum vibration speed is $\sim 21 cm/s$. To drive this point home, one should remember that the anisotropic effect on the coolant cross sections, which moves with speeds of meters per second, is always neglected in reactor physics.

fission source remains constant. Each dynamic eigenvalue iteration consists of the solution of the kinetic equations at the N times $\{t_k, k = 1, \cdots, N\}$. See Sec. 4 for details.

Therefore, our noise kinetic equation reads

$$\left(\frac{1}{v} d_t \psi\right)(\cdots, t) = (\mathcal{B}_{k_D} \psi)(\cdots, t) \tag{10}$$

where $\mathcal{B}_{k_D}$ is the transport operator with the total production term, including prompts and delayed neutrons, divided by the dynamic eigenvalue k_D and where the '$\cdots$' denotes the spatial, angular and energy coordinates. Note that the time partial derivative has been replaced by the material derivative, according to our choice of using a Lagrangian reference frame. For the time discretization we apply an implicit scheme where the right-hand-term in Eq. (10) is computed at the discretization time t_k while the time derivative is typically approximated by a backward step formula involving the precedent time t_{k-1}. However, in this work we have instead used a two-point symmetric finite differences approximation,

$$(d_t \psi)(\vec{r}, \cdots, t_k) \approx \frac{\psi(\vec{r}_{t_{k+1}}, \cdots, t_{k+1}) - \psi(\vec{r}_{t_{k-1}}, \cdots, t_{k-1})}{2\Delta} + O(\Delta^2), \tag{11}$$

where the '$\cdots$' denotes now the angular and energy coordinates and $\vec{r}_{t_{k\pm1}}$ are the positions at times $t_{k\pm1}$ of the point at location $\vec{r}$ at time t_k. As noted, this difference formula is $O(\Delta^2)$, while the usual backward formula is only $O(\Delta)$. It requires, however, knowledge of the flux at the posterior time t_{k+1} but this is not actually a drawback in our numerical solution because we can take advantage of the outer dynamic eigenvalue iterations to get the fluxes $\psi(\vec{r}_{t_{k\pm1}}, \cdots, t_{k\pm1})$ from the previous dynamic eigenvalue iteration. The computation of the material derivative is greatly simplified thanks to our having adopted a Lagrangian mesh that moves with the same velocity that the Lagrangian reference frame. Indeed, the fact that in the Lagrangian frame the position of the spatial points used to estimate the derivative are *time* dependent ($\vec{r}_t$) together with the fact that the spatial discretization mesh is moving along the reference frame, makes the fluxes belong to the same spatial region which occupies different positions over time.

Another approximation we have introduced in the calculation of the time derivative is to compute the angular fluxes that appear in Eq. (11) using a finite-order P_N expansion,

$$\psi(\vec{r}_{t_{k\pm1}}, E, \vec{\Omega}, t_{k\pm1}) \approx \sum_{order(l) \leq L} A_l(\vec{\Omega}) \phi_l(\vec{r}_{t_{k\pm1}}, E, t_{k\pm1}), \tag{12}$$

instead of using the actual fluxes along the trajectories, as a strict application of the method of characteristics would require. In this equation, the $A_l(\vec{\Omega})$ denotes spherical harmonics and the $\phi_l(\vec{r}_{t_{k\pm1}}, E, t_{k\pm1})$ are the associated angular flux moments. The sum over l is done for all spherical harmonics of order smaller or equal to L. A detailed description of the real spherical harmonic implementation in TDT can be found in Sanchez et al. (2002). The reason why we have introduced this seemingly harsh approximation is to avoid a complicated implementation that would have required keeping track in time of the different angular fluxes along the set of trajectories. Moreover, the relevance of the time derivative term clearly depends on the chosen period of oscillation: to be consistent with the typical order of magnitude of mechanical vibrations

(Rouchon, 2016), a frequency of 1 Hz has been considered within the simulation ($T = 1$ s). It has been verified that for such a value the flux derivative with respect to time produces no significant effect on the global source and hence could be neglected. Nevertheless, to maintain the full generality of our approach, we have kept this term in our calculations. Due to this fact, in this work we have limited our consideration to the second-order finite difference scheme of (11), even if higher order schemes could have been used.

We conclude this section by noting that introducing Eq. (3) into (2) gives rise to a problem only based on the neutron flux, which can therefore be treated independently of precursor evolution. This is what we have done here and in the following.

3. FROM ISOTOPIC TO MACROSCOPIC DYNAMICAL CROSS SECTIONS

In this section we will make a step back with respect to the general theory presented in Sec. 2. Here we will deal with the strategy that has to be adopted to correctly define the macroscopic cross sections that appear in Eqs. (1) and (2). Indeed, traditionally the neutron kinetic problem is written as a function of the neutron flux plus a given number of neutron precursor families (typically 6 or 8). Of course these families are model artifacts and do not own direct nuclear data, in terms of emission densities or fission cross sections. These latter have to be reconstructed from isotopic data present in nuclear data files. This procedure entails some necessary flux weighting strategy. We beleive that the strategy, we propose in this section, is less heuristic than the typical approach of using a representative infinite medium to compute a weighting flux.

3.1. General problem definition

When looking at the nuclear data stored in the library one is obliged to express the fission operator, $\mathcal{F}$, carefully separating the two contributions given by the prompt and delayed fission:

$$\begin{aligned}(\mathcal{F}\phi)(\vec{r},E,t) = &\sum_{j=1}^{N_f}\sum_{M=1}^{MG}\chi^p_{j,M}(E)\int_{E_M}dE'\big(1-\sum_{i=1}^{N_{delayed}}\beta_i^j(E')\big)(\nu\Sigma_{f,j}\phi)(\vec{r},E',t)\\ &+\sum_{j=1}^{N_f}\sum_{i=1}^{N_{delayed}}\chi_i^{d,j}(E)\lambda_i^j C_i^j(\vec{r},t),\end{aligned} \tag{13}$$

where we have used the following definitions:

$\beta_i^j(E')$**:** energy dependent fraction of delayed neutrons emitted by precursors of the i-th family produced by the isotope j. We will note also $\beta^j = \sum_{i=1}^{N_{delayed}}\beta_i^j(E')$, which is the quantity appearing in (2).

$C_i^j(\vec{r},t)$**:** delayed precursor concentration of the i-th family in provenance from the isotope j at position $\vec{r}$ and time t.

λ_i^j**:** decay constant of precursors of the i-th family produced by fission of the j-th fissile isotope.

We note that to put the previous recommendations into work we can take into account that

$$\beta_i^j(E') = w_i^j P_{ed}^j(E'), \tag{14}$$

where $P_{ed}^{j}(E')$ is the energy distribution of the yield that depends only on the isotope, not on the precursor family. Note that (14) represents exactly what can be found in nuclear data files such as JEFF (Santamarina et al., 2009) which we use in this work, and for this reason including it in the following is not a supplementary complication. Defining $\overline{w}^{j} = \sum_{i=1}^{N_{delayed}} w_i^j$, one can then find that

$$\beta^j = \overline{w}^j P_{ed}^j(E'), \tag{15}$$

which is the quantity to be substituted into Eq. (2). The evolution equation for the concentration of precursors produced by isotope j and belonging to the i-th family is

$$\partial_t C_i^j(\vec{r},t) = -\lambda_i^j C_i^j(\vec{r},t) + \int_E dE' \beta_i^j(E')(\nu\Sigma_{f,j}\phi)(\vec{r},E',t), \tag{16}$$

where we insist on the energy dependence of β_i^j, which is physically justified but seldom presented in literature. In order to compute a manageable kinetic problem the assumption is made to express the problem as a function only of the total number of precursors per family:

$$C_i(\vec{r},t) = \sum_{j=1}^{N_f} C_i^j(\vec{r},t). \tag{17}$$

To insert this quantity into (13) we define the average emission density per delayed-neutron family

$$\bar{\chi}_i^d(\vec{r},E,t) = \frac{\sum_{j=1}^{N_f} \chi_j^{d,i}(E)\lambda_i^j C_i^j(\vec{r},t)}{\sum_{j=1}^{N_f} \lambda_i^j C_i^j(\vec{r},t)} \approx \frac{\sum_{j=1}^{N_f} \chi_j^{d,i}(E) C_i^j(\vec{r},t)}{\sum_{j=1}^{N_f} C_i^j(\vec{r},t)}, \tag{18}$$

where now a parasitic space and temporal dependence has appeared in the emission density, and also the average decay constant

$$\bar{\lambda}_i(\vec{r},t) = \frac{\sum_{j=1}^{N_f} \lambda_i^j C_i^j(\vec{r},t)}{\sum_{j=1}^{N_f} C_i^j(\vec{r},t)} \approx \lambda_i, \tag{19}$$

where again space and time are introduced by the homogenization procedure. It has to be noted that in the 8-group precursor family definition the decay constants have values that are almost independent of the fissile isotope. This amply justifies the approximated equalities in the previous two equations, and in particular that the decay constants in Eq. (19) are homogenization independent. By making use of all this, one can write the delayed fission integral as:

$$F_d\vec{C} \approx \sum_{i=1}^{N_{delayed}} \bar{\chi}_i^d(\vec{r},E,t)\lambda_i \sum_{j=1}^{N_f} C_i^j(\vec{r},t) = \sum_{i=1}^{N_{delayed}} \bar{\chi}_i^d(\vec{r},E,t)\lambda_i C_i(\vec{r},t). \tag{20}$$

Similarly we can define an average yield per precursor family:

$$\bar{\beta}_i(\vec{r},t) = \frac{\sum_{j=1}^{N_f} \int_E dE' \beta_i^j(E')(\nu\Sigma_{f,j}\phi)(\vec{r},E',t)}{\sum_{j=1}^{N_f} \int_E dE'(\nu\Sigma_{f,j}\phi)(\vec{r},E',t)}, \tag{21}$$

which shows how the family delayed fraction is function of the isotope fission cross sections, the neutron flux and the isotope yields. Even inside blocks of homogeneous media, this spatial variation cannot formally

be neglected if one aspires to obtain a precise calculation. However, it seems to be customary in kinetic calculations to neglect this dependence. On the other hand, delayed emission densities have an isotopic dependence which is not negligible, but not even blatant. Using definition (21) we can finally arrive at Eq. (1).

In conclusion of this sub-section, we remark that the classical kinetic problem, defined by the system of Eqs. (1) and (2), entails the calculation of data per *precursor family*, as given by Eqs. (18) and (21)), which in turn are function of the searched solution. This problem presents an average on isotopes and a weighted energy condensation, and therefore it needs an iterative strategy, which can certainly take advantage of the presumably weak dependence of the *precursor family* data from the isotopic mixture.

3.2. Iterative strategy

In the mild kinetic conditions that are typical of noise problems (where a small deviation is present around an average value) a presumably optimal model flux should be the critical one. And in fact in our experience for noise problems we have not found any noticeable effect in the use of the direct temporal flux. For more severe kinetic problems, it is known (Dugan et al., 2016) that using more faithful model fluxes for the weighting procedure is mandatory. In any case we will suppose that a good starting point is the critical equilibrium flux $\phi^{crit} = \int_{4\pi} d\vec{\Omega}\psi^{crit}(\vec{r},\vec{\Omega},E)$, where ψ^{crit} is solution of the critical problem:

$$\mathcal{L}\psi^{crit}(\vec{r},\vec{\Omega},E) = \mathcal{H}\psi^{crit}(\vec{r},\vec{\Omega},E) + \frac{1}{k_{eff}} \sum_{\substack{j=1,N_f \\ M=1,MG}} \chi^T_{j,M}(E) \int_{E_M} dE'(\nu\Sigma_{f,j}\phi^{crit})(\vec{r},E'), \tag{22}$$

where k_{eff} is the multiplication factor. The equilibrium concentrations are then given by

$$C_i^{j,crit}(\vec{r}) = \frac{\int_E dE'\beta_i^j(E')(\nu\Sigma_{f,j}\phi^{crit})(\vec{r},E')}{\lambda_i^j}. \tag{23}$$

Starting from these values, we will consider that emissions are constant in time and that yields can be updated with (21). It is important to note that $\chi^T_{j,M}(E)$, which is the total emission spectrum for static calculation (and which is classically used in reactor calculation), is not defined by nuclear data. It has therefore to be expressed by a homogenization procedure, like the one that will be discussed in the following. Having solved for the flux we can eventually insert Eq. (1) into Eq. (18) to test convergence, but in our problems this test has never failed. In other words, for our experiences in noise problems, we have never found that a *dynamical* or temporal dependence in the kinetic parameters is important. We suppose that this is due to the *mild* conditions that characterize the noise kinetics, which never move too far from criticality.

To resume, we can say that in our numerical implementation we loop back until convergence between fluxes and precursor concentrations and macroscopic homogenized delayed data during the kinetic simulation. Nevertheless, in our experience, the values obtained by the first *static* case converge very fast. When compared to the *external library* value, the *locally* condensed (18), (19) and (20) can present significant differences. Since in our calculations we use an eight family delayed library, we have fixed decay constants. Nevertheless we remark that with a six family delayed library these constants are isotope dependent. On the

contrary, yields are sufficiently different between isotopes to generate a true coupling and, therefore, result in a truly heterogeneous field of values. To be noted that these yields (or β values) bear almost constant values in the thermal-energy range, while their isotopic dependence becomes relevant in the fast domain.

In our implementation, the fact that the loops are really performed or not, is left to the user decision, but we believe to be of primary importance to be able to underweigth the approximation. For example, let us retrieve simply in stationary conditions the relation between the total emission spectrum and the prompt and delayed spectra for a given isotope. Using Eq. (13), after inserting in it the values of Eq. (23), gives

$$\chi^T_{j,M}(\vec{r},E) = \chi^p_{j,M}(E)(1-\bar{\beta}_{j,M}(\vec{r})) + \sum_{i=1}^{N_{delayed}} \chi^{d,i}_j(E)\beta^j_{i,M}(\vec{r}). \tag{24}$$

where $\bar{\beta}_{j,M}(\vec{r}) = \sum_{i=1}^{N_{delayed}} \beta^j_{i,M}(\vec{r})$ and

$$\beta^j_{i,M}(\vec{r}) = \frac{\int_{E_M} dE' \beta^j_i(E')(\nu\Sigma_{f,j}\phi)(\vec{r},E')}{\int_{E_M} dE'(\nu\Sigma_{f,j}\phi)(\vec{r},E')} \tag{25}$$

is the average delayed fraction per isotope, macro-group and family.

In the general case, it can be useful that different spatial regions could share the same macroscopic cross section. If we define a *medium* as being the identifier of a macroscopic cross section, a per-medium quantity f_{MEDIUM} can be evaluated as $\int_{MEDIUM} d\vec{r}\, f(\vec{r})/V_{MEDIUM}$, where V_{MEDIUM} is the total volume of the medium being considered, that is, the sum of the volumes of the regions containing that medium. This is valid for $\chi^T_{j,M}(\vec{r},E,t)$ of Eq. (24) and $\bar{\chi}^d_i(\vec{r},E,t)$ of Eq. (18). Moreover, Eq. (24) shows that, even in the stationary critical problem, the spectrum should depend on the solution. Quite strangely no one, to our knowledge, includes this dependence in its equations, with the second term on the right-hand side of the equation (24) being estimated *a priori*. Of course, when kinetic situations are taken into account, weighting fluxes for βs or precursor concentrations for χs are not to be assumed nearly critical, and important spectral and spatial shifts can lead to sensible changes in macroscopic cross sections. We believe that this point needs to be verified.

We note that, under the classical approximation, the βs values are computed by supposing to have a uniform spatial independent model flux ϕ in Eq. (25). This approach is acceptable only for energy ranges where the $\beta^j_i(E)$ can be considered energy independent or in cases where there are not important spatial variation of the energy flux spectrum.

In conclusion we have brought to the solvers TDT and IDT (Masiello et al., 2009) of APOLLO3® the λ and β quantities of the kinetic problem up to their fission iteration routines. And this not only for the kinetic problem itself, but also for the stationary one, since, as shown in Eq. (24), some effects could be theoretically found due to this functional dependence even in stationary calculations. Once these quantities are available, one can easily implement the local modifications of spectra during sweep to include the coherent formula (24) (if one is only interested in a static calculation) or also the kinetic parameters given by Eqs. (21) and (18) (for dynamic calculations).

3.3. Remarks on data structure

Eq. (14) shows that some storage can be avoided and that the following more efficient formula, derived from (24), can be adopted:

$$\chi^T_{j,M}(\vec{r},E) = \chi^p_{j,M}(E)\frac{\int_{E_M} dE' \left(1-\overline{w}^j P^j_{ed}(E')\right)(\nu\Sigma_{f,j}\phi^{crit})(\vec{r},E')}{\int_{E_M} dE'(\nu\Sigma_{f,j}\phi^{crit})(\vec{r},E')} + \bar{\chi}^d_j(E)\frac{\int_{E_M} dE' P^j_{ed}(E')(\nu\Sigma_{f,j}\phi^{crit})(\vec{r},E')}{\int_{E_M} dE'(\nu\Sigma_{f,j}\phi^{crit})(\vec{r},E')}, \quad (26)$$

where $\bar{\chi}^d_j(E) = \sum_{i=1}^{N_{delayed}} \chi^{d,i}_j(E) w^j_i$. This last formula asks for some comments. Consider for example a hypothetical case where $P^j_{ed}(E)$ (as it is generally the case) increases as energy decreases and arrives at saturation for all energies below 300 keV. If we then consider the case of very fast spectrum reactors, where the average neutron energy can be of 600 or 500 keV, we can reasonably expect the $\int_{E_M} dE' P^j_{ed}(E')(\nu\Sigma_{f,j}\phi^{crit})(\vec{r},E')/\int_{E_M} dE'(\nu\Sigma_{f,j}\phi^{crit})(\vec{r},E')$ factor to be quite smaller than unity. This implies that the impact of this weighting can strongly depend on the flux. The usual procedure is to employ model fluxes, obtained in an infinite medium calculation or supposed to be representative of a heterogeneous cell-level system. We believe that it is important to have the possibility of directly using the assembly-level fluxes in Eq. (26), which in our opinion are closer to the physics, to at least be able to mesure the error of the standard approximation.

3.4. Some tests on static assembly calculations

The formalism proposed in this section is not limited to kinetic calculations but can already be used in classical critical calculations and tested against the usual approach of a pre-calculated total fission spectrum per isotope. In this sub-section we propose to show some results in order to understand if our approach is reasonable and if can be effective. Since the main goal of the paper is to deal with neutron noise we will not make extensive comparisons, leaving it to future works. The APOLLO3® one-eigth assembly calculations shown in this section have been compared to the Monte-Carlo code TRIPOLI-4® (Brun et al., 2015), with respect to which we show reactivity and fission-rate errors. Both TRIPOLI-4® and APOLLO3® have used a JEFF cross section library (Santamarina et al., 2009), and the latter has employed a 281 group energy mesh (Hfaiedh and Santamarina, 2005). On the other hand, the APOLLO3 calculations have been done with 4 macro fission spectra, that is to say with $MG = 4$ in Eq. (2). As explained in Sec. 3.3, the main advantage in using Eq. (26) is supposed to appear for cases where the neutron spectrum is affected by strong thermal absorptions. For this reason we have chosen to show two rodded assembly calculations with AIC BC4 rod pins. For the former we show, in Fig. 1 the computational mesh and the layout of shielding media, that for our cases have been differentiated per each cell. This is to be as precise as permitted by our deterministic model. For the other assembly a similar computational scheme has been adopted. Results are shown in Tab. 1. As expected, from the comments made in Sec. 3.3, the reactivities are increased by

Table 1: Comparison Tripoli-4 and APOLLO3 reactivity values for cases with *standard* fission spectra or *local* weighted ones.

		APOLLO3 reactivities results	
	Tripoli-4	**standard spectrum**	**local spectrum**
B4C Assembly	0.55130	0.54981	0.55264
AIC Assembly	0.59839	0.59550	0.59834

the use the *local* model, which is benefical in the cases we show here. Of course a detailed comparison in an ample range of cases is mandatory, before arguing if this technique can be retained in general for reactor physics calculations. But this is beyond the scope of the present work. Nevertheless we think that Tab. 1 shows that the weight of this model is far from being negligible, which can be of interest for the scientific community.

4. ITERATIVE ALGORITHM, LEAKAGE AND SELF-SHIELDING

One of the mandatory conditions to simulate a periodic behavior of a fissile system, in order for the physical quantities to be periodic, is that the system has to be critical on the average, that is, it has to keep the net neutron balance constant from a period of oscillation to the next. For this purpose a dynamic eigenvalue is introduced in the time-dependent transport equation:

$$\big((\frac{1}{v}d_t + \mathcal{L} + DB^2 - \mathcal{H})\psi\big)(t) = \frac{1}{k_D}(\mathcal{F}\phi)(t), \tag{27}$$

where $(\mathcal{F}\phi)(t) = (\mathcal{F}_p\phi + \mathcal{F}_d\phi)(t)$ represents the total production term including both prompt and delayed neutrons. The term DB^2, needed to achieve the initial criticality, is computed when the system is in the unperturbed condition by means of a homogeneous leakage model (Sanchez, 2002) available in APOLLO3®, and then employed for the rest of the simulation. For completeness, In appendix A we summarize the basic equations of the leakage theory that we use here and some implementation details relative to its application to noise calculations.

The dynamic eigenvalue k_D calculation is based on the condition that

$$\int_0^T dt < \mathcal{F}\phi(t) > \; = \|\mathcal{F}\phi\|_{0,T} = \|\mathcal{F}\phi\|_{T,2T} = \cdots = constant, \tag{28}$$

where '$< \cdots >$' represents the integration over space, angle and energy, so that $\|\mathcal{X}\|_{0,T}$ represents a full phase space integration with only a limited temporal domain integration in $0,T$. Condition (28) implies that the integral of the fission source over a period is to be independent of the chosen periodic interval. Similarly to the classical power-iteration method, the dynamic eigenvalue is updated as the ratio between the current

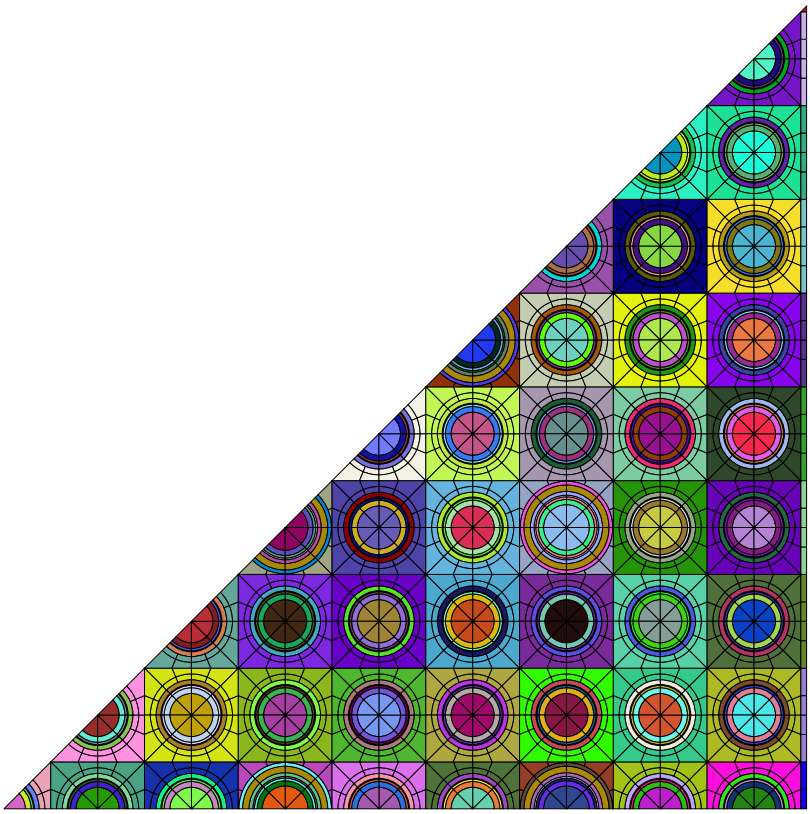

Figure 1: Computational mesh of the rodded AIC assembly. As indicated by the color display all cells have been indipendently self-shielded, in order to grant a maximum degree of precision.

fission source and the normalized previous one; fulfilling condition (28) requires however to consider time

integrals of the source:

$$k_D^n = \frac{\int_T dt < \left(\mathcal{F}\vec{\phi}^n\right)(t) >}{(1/k_D^{n-1}) \int_T dt < \left(\mathcal{F}\vec{\phi}^{n-1}\right)(t) >} \approx \frac{\sum_{k=1}^N < \left(\mathcal{F}\vec{\phi}^n\right)(t_k) >}{(1/k_D^{n-1}(\sum_{k=1}^N < \left(\mathcal{F}\vec{\phi}^{n-1}\right)(t_k) >}. \tag{29}$$

In the expression above $\left(\mathcal{F}\vec{\phi}\right)(t)$ is the total source evaluated at time t and the vector notation for the flux suggests the dependence of this term on the whole period. The time integrals are approximated by constant-weight sums. We can anticipate that in the final iterative form of Eq. (29) we will use the delayed source instead of the total one. This will be discussed in the next section. The dynamic eigenvalue here defined plays the role of a fictitious feedback: periodicity could be guaranteed by an external feedback as, for instance, a certain boron concentration to be determined iteratively; in that case, the dynamic eigenvalue would simply be equal 1.

4.1. Dynamic eigenvalue update

Even if starting from a critical condition, neutron noise may be responsible for more or less relevant insertions of reactivity, generally oscillating around a null value. This may lead the number of fission reactions to diverge or to decrease progressively up to be negligible, depending on the value of the average reactivity along a period; however, even if this value is equal to 0, the presence of delayed neutrons may be the promoter of system divergence, as described for a point reactor in Ravetto (1997). In our case, in order to preserve an asymptotic periodic behavior, any deviation from an average 0 value for the reactivity is compensated with the dynamic eigenvalue by which the fission source is divided. In the light of section 4 and considering how the k_D is updated after each outer iteration (29), our dynamic eigenvalue takes into account the entire evolution of the system during the period and is therefore suitable for this task. Figure 2 shows the algorithm that we have adopted for computing and updating until convergence of the dynamic k_D and the fission source values over time. For the former, the relative error between successive iterations has to be less or equal to 10^{-5}, whereas for the latter the maximum acceptable value for the relative error over the period has been set to $2.0\ 10^{-4}$.

The implemented noise simulation consists in an iterative cycle external to the power method outer iterations. At the beginning of each "noise" iteration (index n) the delayed fission source is fixed along the entire period; then, for each time sub-interval k, the following fixed-source problem is solved:

$$\left(\hat{\mathcal{L}} - \mathcal{H}\right)\psi^{n,o}(t_k) - \frac{1}{k_D^{n-1}}\mathcal{F}_p\phi_0^{n,o-1}(t_k) = \frac{1}{k_D^{n-1}}\mathcal{F}_d\phi_0^{n-1}(t_k) + S^{n-1}\phi(t_k), \tag{30}$$

where the o index stands for *outer* iteration on *prompt* fission, $\hat{\mathcal{L}} = \mathcal{L}+DB^2$ and $S^{n-1}\phi(t_k) = \sum_l A_l[\phi_l^{n-1}(\vec{r}_{t_{k+1}}, E, t_{k+1}) - \phi_l^{n-1}(\vec{r}_{t_{k-1}}, E, t_{k-1})]/(2v\Delta)$ is the time derivative term. If k_D is not too far from 1, in particular if its value is lower than the static eigenvalue by an amount that is smaller than the delayed-neutron fraction of the set of fissile isotopes considered, then problem (30) is expected to converge. The algorithm requires to find the flux solutions of the N sub-intervals in order to update the delayed source and the dynamic eigenvalue (in Eq. (29)) for the next noise iteration.

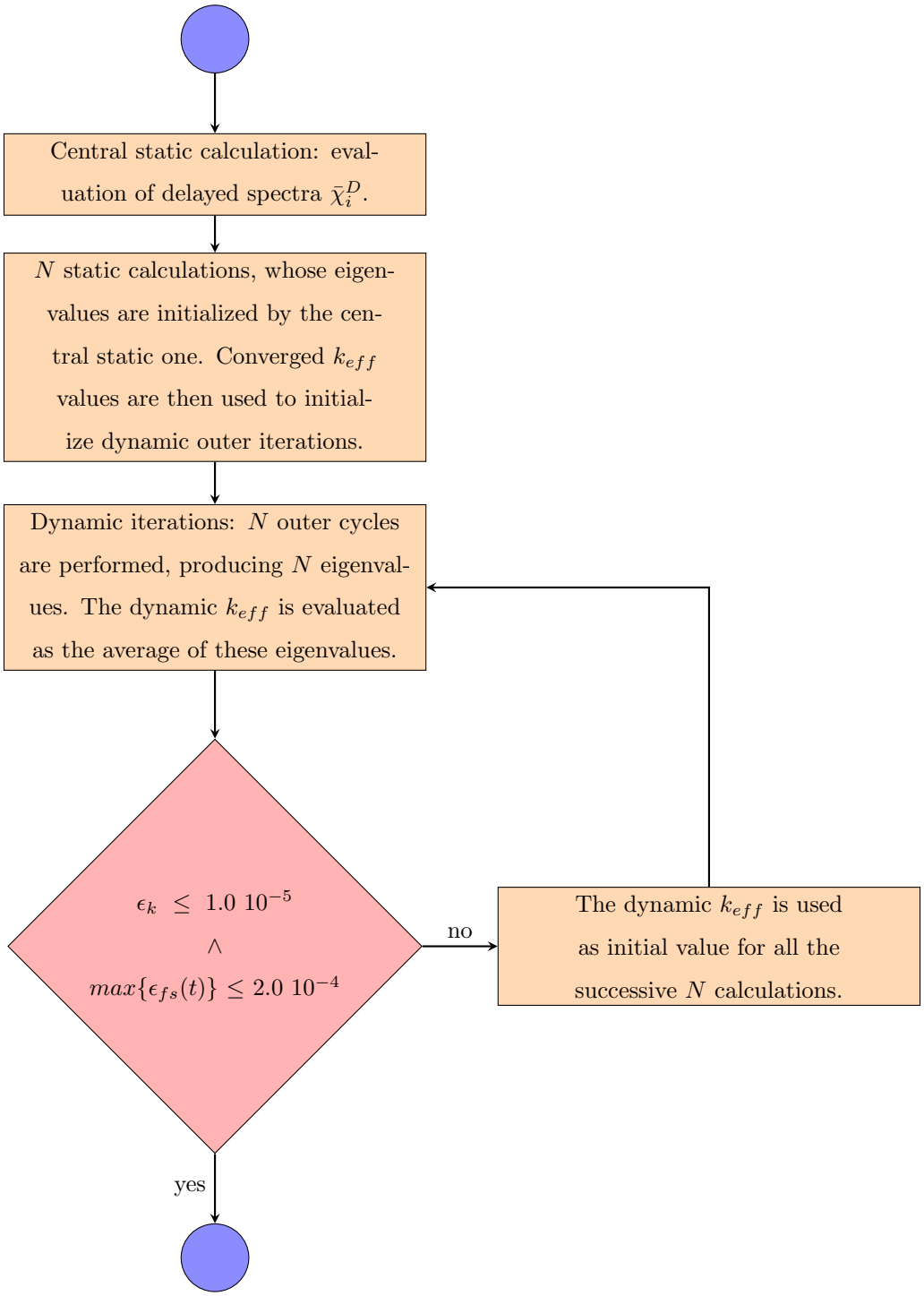

Figure 2: Algorithm for noise iterations. ϵ_k **and** ϵ_{fs} **are the relative errors between successive iterations of the dynamic** k_{eff} **and of the fission sources** $< \mathcal{F}(t)\phi(t) >$**, respectively. For the latter, the maximum value over the period is considered to check convergence.**

4.2. Wielandt-type scheme for outer iterations

In this paragraph we want to discuss the fact that Eq. (30) can be viewed as a sort of Wielandt scheme.

The meaning of the dynamic eigenvalue k_D for our kinetic problem has been discussed in 4.1; from now on, it will be referred to simply as k. Considering the eigenvalue problem

$$\mathcal{A}\phi = (\mathcal{M}^{-1}\mathcal{F})\phi = k\phi \iff \mathcal{M}\phi = \frac{1}{k}\mathcal{F}\phi, \tag{31}$$

having exactly the same form as (30), once the time derivative terms have been neglegted, which is what we will suppose here to simplify the presentation. The number of power iterations to reach the convergence of the fundamental eigenvector depends on the so-called "dominance ratio" σ, equal to the ratio k_2/k_1 of the two highest eigenvalues k_2 and k_1 of matrix $\mathcal{M}^{-1}\mathcal{F}$ (k_1 being the fundamental one). In particular, the smaller σ the faster the convergence. As proposed for example in Kochunas et al. (2017), the value of the dominance ratio can be reduced by means of an eigenvalue shift, modifying the original problem as follows:

$$\left(\mathcal{M} - \frac{1}{k_s}\mathcal{F}\right)\phi = \left(\frac{1}{k} - \frac{1}{k_s}\right)\mathcal{F}\phi. \tag{32}$$

This procedure is called Wielandt shift method, and in order for the shift to be effective k_s must be greater than k_1: in this way the new dominance ratio, given by $\sigma' = (\frac{1}{k_1} - \frac{1}{k_s})/(\frac{1}{k_2} - \frac{1}{k_s})$ is surely smaller than the initial one. In our work a sort of Wielandt scheme has been implemented by subtracting the prompt source from both sides of (27) to write (30). The resulting iterative equation (on the dynamical index n) is therefore

$$\left(\hat{\mathcal{L}} - \mathcal{H}\right)\psi^n(t_k) - \frac{1}{k_d^{n-1}}\mathcal{F}_p\phi^n(t_k) = \frac{1}{k_d^{n-1}}\left(\mathcal{F}_d\vec{\phi}^{n-1}\right)(t_k) + S\phi^{n-1}(t_k), \qquad k = 1, N. \tag{33}$$

Table 2: Geometry and oscillation data

Dimensions	[cm]
Cell side	1.26502
Guide tube inner radius	5.72379 10^{-1}
Detector anode radius	1.50000 10^{-1}
Detector cathode outer radius	2.00000 10^{-1}
Detector envelope outer radius	2.80000 10^{-1}
Detector shift amplitude	$\pm$2.60000 10^{-1}
Control-rod cladding radius	4.86125 10^{-1}
Rod bundle shift amplitude	$\pm$8.00000 10^{-2}

Equation (33) implies the inversion of the operator $\mathcal{M} = \hat{\mathcal{L}} - \mathcal{H} - \frac{1}{k^{n-1}}\mathcal{F}_p$ whose first eigenvalue is approximately reduced with respect to the critical static one by the fraction of prompt neutrons ($\sim 99.4\%$ for thermal systems). If, after a suitable initialization, our iterative scheme is over this limit and if the reactivity oscillation due to the noise is small compared to the difference between total and prompt sources (around 600pcm), our fictitious k_s is always greater than the prompt static eigenvalue and the previous scheme can be considered safe. In contrast to the standard Wielandt scheme, our procedure will not reduce the dominance ratio, even if transferring all the prompt fission onto the k-th step inversion should reduce the iterations on the time steps. Finally our scheme can be written:

$$\psi^n(t_k) = \mathcal{M}^{-1}\big[\frac{1}{k_d^{n-1}}\big(\mathcal{F}_d\vec{\phi}^{n-1}\big)(t_k) + S\phi^{n-1}(t_k)\big], \qquad k = 1, N. \tag{34}$$

To update the dynamic eigenvalue the condition is to re-scale the delayed emission with the help of the estimated eigenvalue as

$$k^n = k^{n-1}\frac{\|\mathcal{F}_d\vec{\phi}^n\|}{\|\mathcal{F}_d\vec{\phi}^{n-1}\|}, \tag{35}$$

where the norm notation of Eq. (28) has been used. Moreover it has to be noted that the final *practical* formula for eigenvalue update is different from the initial Eq. (29).

4.3. Temporal noise spatial integration with Sanchez Lagrangian approach

The main goal of this section is to comment the technique used to discretize the temporal movement of the noise vibration. We have in fact used an approach consisting in *following* the geometrical displacement of fissile pins with a lagrangian approach. This strategy is in the footsteps of a recent work of Dr. Sanchez (2015), from whom we borrow a great part of the following notation. Therefore, following this author, we call D and D_0 the global system and the part of it subject to geometrical deformations or material changes, respectively. We can now introduce the basic *noise* geometrical transformation:

$$\begin{aligned} \pi_t &: D_0 \to D_t \\ \vec{r} &= \pi_t(\vec{r_0}) \end{aligned} \tag{36}$$

which continuously transforms the initial spatial domain (at time 0) into the deformed one at time t. At this point the expressions of the derivative terms of (1) require some comments: in principle, instead of partial derivatives one should refer to material ones, given by:

$$d_t f(\vec{r}, t) = \partial_t f + \vec{v}\cdot\nabla f. \tag{37}$$

This approach can be found in Dulla et al. (2004). However, as noted in Sanchez (2015), the full material derivative of a generic function f can be expressed more easily by considering the function $\hat{f}(\vec{r_0}) = f(\pi_t(\vec{r_0}), t)$, so that:

$$d_t f(\vec{r},t) = \partial_t \hat{f}. \tag{38}$$

The strategy for a lagrangian approach is therefore paved: a suitable MOC discretization is constructed at time 0, and then *propagated* continuously for the other times. Then, for both fluxes and precursor concentrations the *hat* functions described above are considered and, for the latter, the partial derivative of the type (38) is used into the equations (the reader has to keep in mind that in fact they are consistent with the material derivative of type (37) of the classical eulerian discretizations). Fig. 3 shows some examples of the spatial discretizations we have used in our studies.

4.4. Self-Shielding treatment

For a general description of the self-shielding techniques available in APOLLO3® we refer the reader to Mao et al. (2019). Here we will only insist on some peculiarities present in the self-shielding treatment of the temporal-domain discretization of the noise problem we have adopted. Referring to Fig. 2, we can say that in our approach we always do the self-shielding treatment for the central static calculation. Using the shielded cross sections of this initial calculation into the other *deformed* ones could imply an approximation that can be tested by undergoing the supplementary self-shielding calculations in the non-static situations. We have tested this convergence in our cases, but we have found that supplementary self-shielding calculations do not lead to changes greater than the margins of the requested precisions in the fluxes and rates. Of course this consideration is case-dependent and it could be possible to have different conclusions for cases where the neutron noise produce higher flux and/or spectral local variations.

Of course a more important *structural* limit of our work is the approximation of using self-shielding techniques that have been conceived and tested for static and critical calcultions into kinetic ones. This fundamental assumption, that we have accepted in this work, has not been tested. Looking at Dugan et al. (2016) one can strongly doubt of the reasonableness of these assumptions for cases where the reactivity is too far from criticality. For cases where the system undergoes only a small perturbation around criticality one can be more confident. But we do not have quantitative arguments to demonstrate that our approach is not questionable. Therefore we leave to future research to examine this point.

5. ACCELERATION METHOD

The iteration scheme described in paragraph 4, can be considered the equivalent of the standard "free iterations" (Adams and Larsen, 2002), and even if placed in the favorable conditions of a Wielandt shift may converge to the solution rather slowly: there is therefore a need to adopt acceleration techniques that can reduce the computational time. For this purpose, two different strategies have been used at once: firstly, a special treatment is reserved to the fission source, due to its expression in our temporal noise problem; secondly, a DP_N synthetic acceleration is implemented. It has to be noted that these techniques apply to

each time step of the noise period: the acceleration of our method is achieved by accelerating the convergence of single time points.

The inner cycles corresponding to the index o are accelerated by means of the DP_N synthetic method (Santandrea, 2007) already implemented in the APOLLO3® code: basically, the last transport solution, referred to as $\psi^{o-\frac{1}{2}}$, is "corrected" by a term $\delta\psi^{o-\frac{1}{2}}$ which is solution of the simplified problem

$$\big(\mathcal{L}_{DP_N} - \mathcal{H}\big)\delta\psi^{o-\frac{1}{2}}(t_k) - \frac{1}{k_D}\mathcal{F}_{\mathcal{P}}\delta\phi^{o-\frac{1}{2}}(t_k) = \frac{1}{k_D}\mathcal{F}_{\mathcal{P}}\Delta\phi(t_k), \tag{39}$$

where the transport operator has been substituted by its DP_N version and the source is now given by the difference between the two latest transport iterates ($\Delta\phi = \phi^{o-\frac{1}{2}} - \phi^{o-1}$). The correction term is then added to retrieve the next iterate:

$$\psi^{o}(t_k) = \psi^{o-\frac{1}{2}}(t_k) + \delta\psi^{o-\frac{1}{2}}(t_k). \tag{40}$$

Full convergence requires to stabilize the delayed-fission sources at every time point k.

5.1. DP_N synthetic acceleration

According to the Wielandt scheme just described, each outer iteration contains within it a further level of fixed-source iterations:

$$\big(\mathcal{L} - \mathcal{H}\big)\psi^{s-f}(t_k) = \frac{1}{k^{o-1}}\mathcal{F}_p\phi^{s-1}(t_k) + S^{o-1}(t_k), \qquad k = 1, N, \tag{41}$$

where the index s denotes the nested iteration level. Provided the initial criticality and because of the prompt-delayed separation, eq. (41) identifies a sub-critical source problem for all time steps: a physical result is therefore expected to be found. For a full transport solution f in the left-hand side of (41) is equal to 0, but to further accelerate our procedure we have coupled it with the synthetic acceleration method implemented in TDT: the DP_N scheme. This technique (Santandrea, 2007) belongs to the family of the synthetic methods (Adams and Larsen, 2002) and it is meant to solve a problem derived from the original one considering also the converged solution, denoted by "∞":

$$\big(\mathcal{L} - \mathcal{H}\big)\psi^{\infty}(t_k) = \frac{1}{k^{o-1}}\mathcal{F}_p\phi^{\infty}(t_k) + S^{o-1}(t_k), \qquad k = 1, N. \tag{42}$$

By indicating with $\frac{1}{2}$ the value of f for the latest transport solution, $\psi^{s-\frac{1}{2}}$, and with

$\delta\phi^{s-\frac{1}{2}} = \phi^{\infty} - \phi^{s-\frac{1}{2}}$ the error affecting the $\big(s-\frac{1}{2}\big)$-th transport iteration ($\delta\psi^{s-\frac{1}{2}}$ for the angular flux),

$\Delta\phi = \phi^{s-\frac{1}{2}} - \phi^{s-1}$ the difference between the current transport solution and the iterate relative to the previous step,

one can subtract Eq. (41) to (42) to obtain

$$\big(\mathcal{L} - \mathcal{H}\big)\delta\psi^{s-\frac{1}{2}}(t_k) - \frac{1}{k^{o-1}}\mathcal{F}_p\delta\phi^{s-\frac{1}{2}}(t_k) = \frac{1}{k^{o-1}}\mathcal{F}_p\Delta\phi(t_k), \qquad k = 1, N. \tag{43}$$

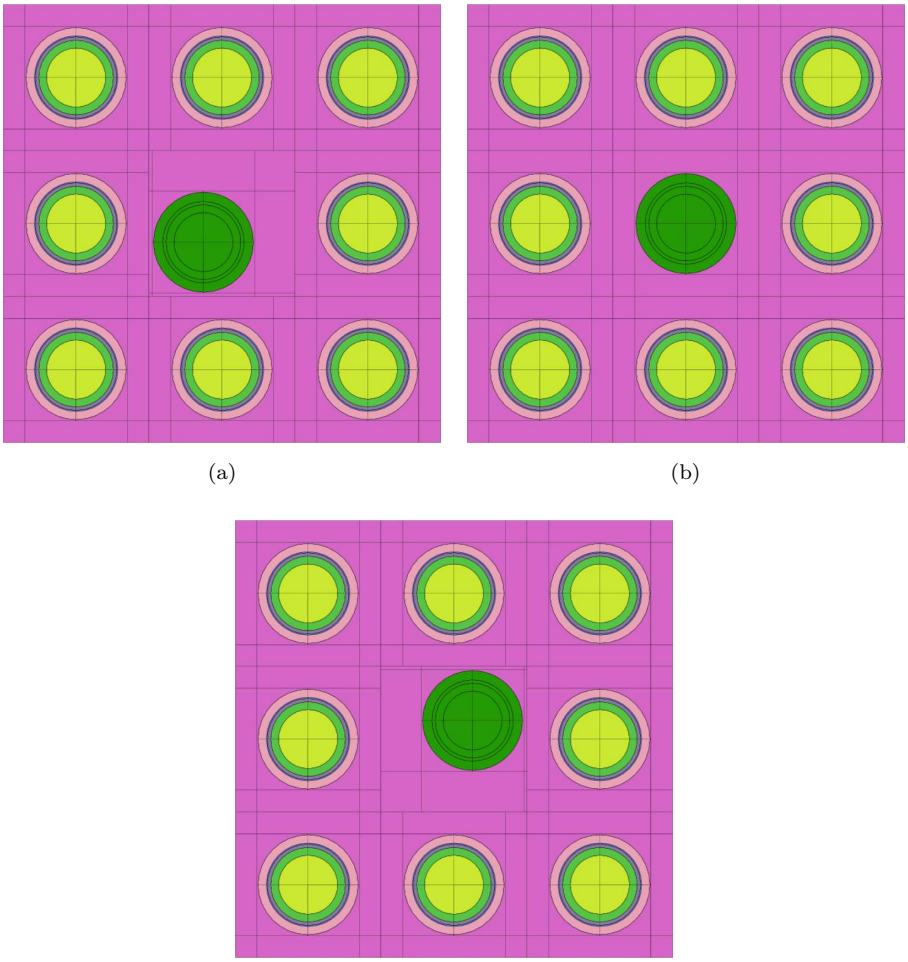

(a) (b)

(c)

Figure 3: Small case for performance comparison. The control rod oscillates along the diagonal of the cell. (a) and (c) are the most distant positions from the centre, which is shown in (b).

Table 3: Comparison free-accelerated. The eigenvalues and the times required by the simulations are shown.

	Iterations	
	free	**accelerated**
Eigenvalue	0.73827	0.73820
CPU time [s]	22621	4978

The aim is to compute $\delta\phi$ and to add it to the latest transport solution in order for the next iterate $\phi^s = \phi^{s-\frac{1}{2}} + \delta\phi^{s-\frac{1}{2}}$ to be a better estimation of the real solution. However, Eq. (43) is as difficult as the original one: as it is, this strategy would not lead to any advantage. The acceleration is therefore made on a simplified problem, where the transport operator $\mathcal{L}$ is replaced by a low-order one, $\mathcal{L}_{DP_N}$. According to Santandrea (2007), this substitution is based on two approximations: the former regards the number of angular moments considered, which is here reduced; the latter treats the region boundary as a set of surfaces, and for the boundary fluxes of each surface only surface-averaged (hence spatially constant) angular moments are used. In this way the chord dependence of the MOC, assuming constant angular fluxes over the cross-sectional area of each trajectory, is lost to the advantage of computational cost. On both surface sides the angular dependence is expressed by means of a P_N spherical-harmonic expansion: hence, a "Double P_N" expansion is adopted, giving the name to the acceleration method.

5.2. Performance comparison

In order to show the effectiveness of the acceleration a small case is considered, whose domain is composed of a 3×3 grid of cells. In the central cell a control rod is present which oscillates as shown in Fig. 3, while the other cells contain fuel. As for the detector and the control-assembly cases, the rod is made of natural boron; the fuel is 1.8% enriched uranium. The side of each cell is 1.28885 cm and the movement of the control rod, which takes place along the diagonal of the cell with a period of 0.2 s, has an amplitude of 0.66178 cm.

In Tab. 3 one can see the converged eigenvalues and the computation times relative to the case of "free iterations" and to the accelerated one. The former differ by less than 10 pcm, which is a rather acceptable quantity, especially considering that the acceleration reduces the simulation time by 78%.

Another interesting aspect of this simple case is to see how the fission integral over the whole domain D, given by

$$I_F(t) = \sum_{j=1}^{N_{isotopes}} \int_D d\vec{r} \int_E dE \; (\nu\Sigma_{f,j}\phi)(\vec{r}, E, t), \tag{44}$$

oscillates along the period: the values are reported in Tab. 4 and plotted in Fig. 4. The amplitude of this variation reaches 56.57% of the average value. However, such a high oscillation is very different from what we

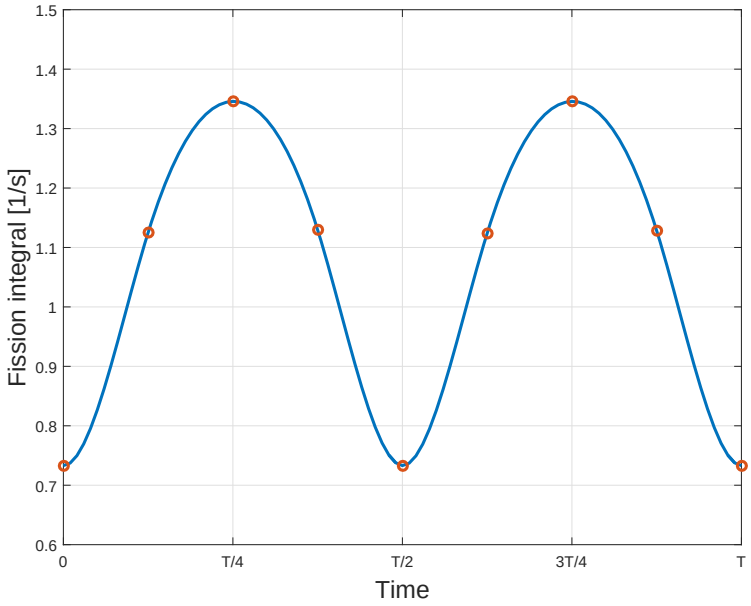

Figure 4: Fission integral oscillation along the period. The red points correspond to the measured values of Tab. 4, which are interpolated by the cubic blue line.

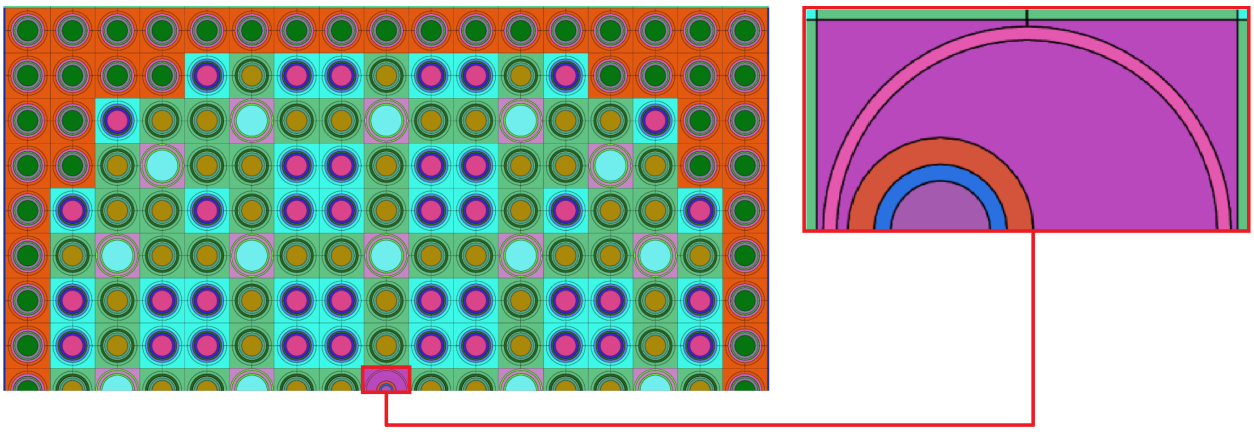

Figure 5: PWR fuel assembly. The halved domain is shown. The fission-chamber detector is inserted in the central cell (the zoom shows its leftmost position).

have obtained for the two main case studies (see Section 6): this might be due to the large difference among the eigenvalues of the static configurations of this case, which alternately produces a relevant insertion of positive and negative reactivities. Table 5 contains these values: clearly, the leakage model discussed in appendix 8 has not been adopted here.

6. CASE STUDIES AND RESULTS

The described method has been implemented for two different 2-D geometries, both involving one or more components oscillating within guide tubes. The movement is supposed to take place horizontally, along the

tube diameter, and in an harmonic fashion. This means that the displacement along the x axis is described by $x(t) = \Delta \cos(\omega t)$ where Δ is the maximal geometrical deformation from the static configuration and ω is the chosen mechanical vibrational frequency. Of course the speed is also harmonic and its maximum value is $\omega\Delta$. If N period sub-intervals are considered, this leads to have $N/2 + 1$ equidistant positions, including the initial one. The use of Silène software (Stankovski, 2011) simplified the geometries construction, making it possible to easily construct non-concentric components (which is essential for simulating the movement of one structure within another). For both cases reflective boundary conditions are assumed, with temperatures equal to 841.00 K in the fuel and to 579.55 K in all other materials. The most relevant geometric data are reported in Table 2.

The first system (Fig. 5) is a 1.8% enriched PWR assembly (17×17) with a fission-chamber detector inside the water tube of the central cell; such an instrument is typically inserted from above, where its unique mechanical constraint is situated, so that given the considerable length of the insertion arm, the detector is likely to swing due to the coolant turbulence. It should be noted that a 2-D representation hardly resembles reality, since the detector length is at least an order of magnitude lower than the fuel assembly; as a consequence, our computed noise effect is probably higher than the physical one.

The other system (Fig. 6) is a cluster of 9 PWR fuel assemblies, arranged on a 3×3 grid, with control rods inserted in the central one. In this case the 2-D model describes quite faithfully the behavior of a mid-height core section, provided that rods be fully inserted, thanks to the weak axial heterogeneity of PWRs. Again, the coolant turbulent motion may induce vibrations of structures and in particular of control rods, as they are constrained only on the top of the assembly. For simplicity, a coherent horizontal oscillation of the whole rod bundle is assumed to take place. Each of the assemblies adjacent to the central one contains 12 pyrex rods and 2.4% enriched fuel, while the enrichment is 1.8% in the others.

For the two cases Table 6 shows the dynamic-eigenvalue results together with the "static" values, which are obtained considering each position along the period independently. The calculations simulate oscillations of 1 Hz using $N = 8$ time sub-intervals and as many positions, with the component(s) starting from the non-oscillation position and moving first up to the leftmost position and then to the rightmost one, before returning to the center. In view of the weak eigenvalue variation among static values, in particular with respect to the delayed-neutron fraction, the algorithm described in Sec. 4 was expected to converge to a dynamic eigenvalue comprised between the maximum and minimum k_{eff}, as it actually did. More interesting results can be found analyzing the variations of fission rates, especially from an industrial perspective, since they directly impact the power output. Denoting by V_i the volume of the general fuel cell i, the fission rate τ_i relative to the same cell can be expressed, as a function of time, as

$$\tau_i(t) = \int_{V_i} d\vec{r} \int_E dE \; (\Sigma_f \phi)(\vec{r}, E, t). \tag{45}$$

As a consequence of the periodic structural oscillation, fission rates acquire a periodic behavior with the same period, attributable to local variations in the moderating ratio. To measure the extent of this effect one can consider, for each cell, the deviations from the average value over the period: identifying the latter as

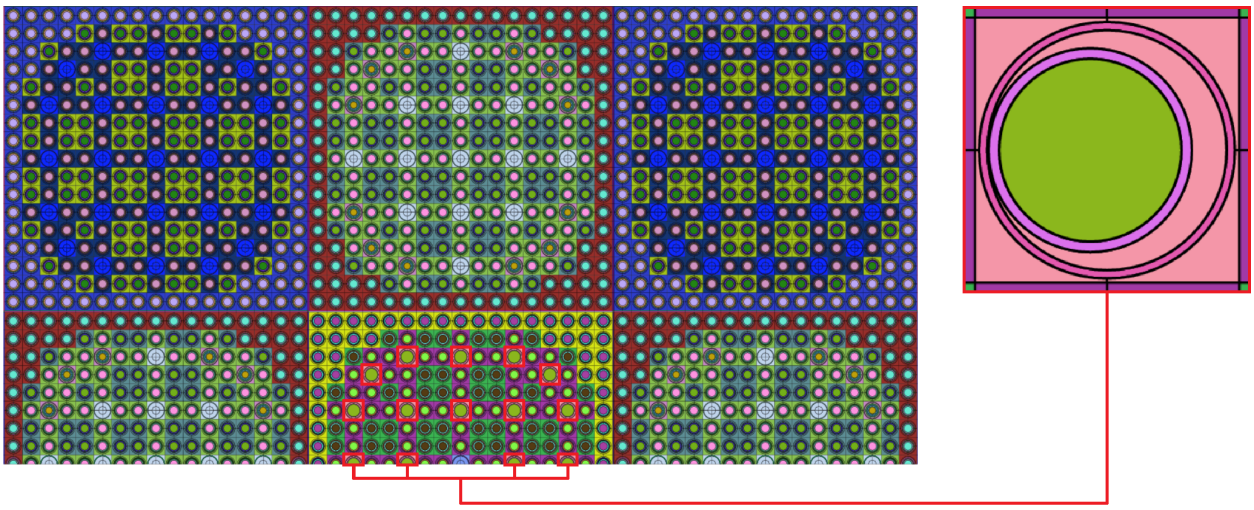

Figure 6: Cluster of 9 PWR fuel assemblies. The halved domain is shown. The moving control rods are in the central assembly (the zoom shows their leftmost position).

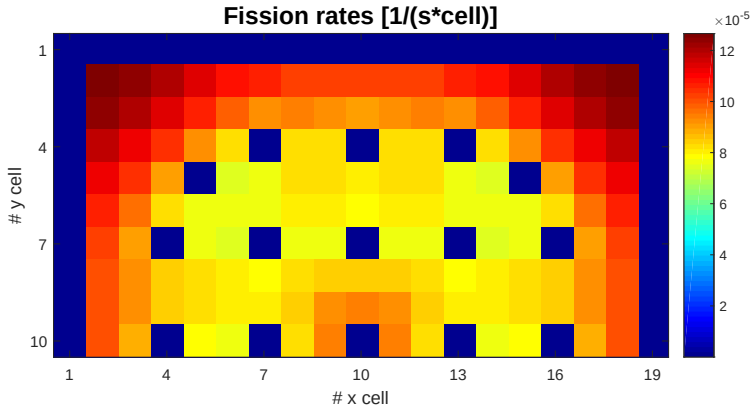

Figure 7: Fission rates for the detector case described in Sec. 6.

$\bar{\tau}_i$ and as τ_i^{max} and τ_i^{min} the maximum and minimum values, respectively, the maximum relative deviation reads

$$\left(\frac{\delta\tau}{\tau}\right)_i = \frac{1}{\bar{\tau}_i} \max\{\mid \tau_i^{\max} - \bar{\tau}_i \mid, \mid \bar{\tau}_i - \tau_i^{\min} \mid\}. \tag{46}$$

This quantity has been chosen to quantify the noise effect, and has therefore been computed and plotted over the whole domain for each case study (Fig. 9).

In Fig. 8 it is possible to appreciate the global layout of fission rates in the cluster. As it could be expected the average rates inside the rodded assembly are much lower than the rest of the bundle. This means that also the absolute noise level (which takes place inside the rodded assembly) is at an absolute low level. Similarly, in Fig. 7 it is possible to look at the fission rates for the case of the detector. Note that in both cases a water gap is explicitly represented, and this gives rise to the *zero* fission rates between assembly or at the boundary of the detector assembly.

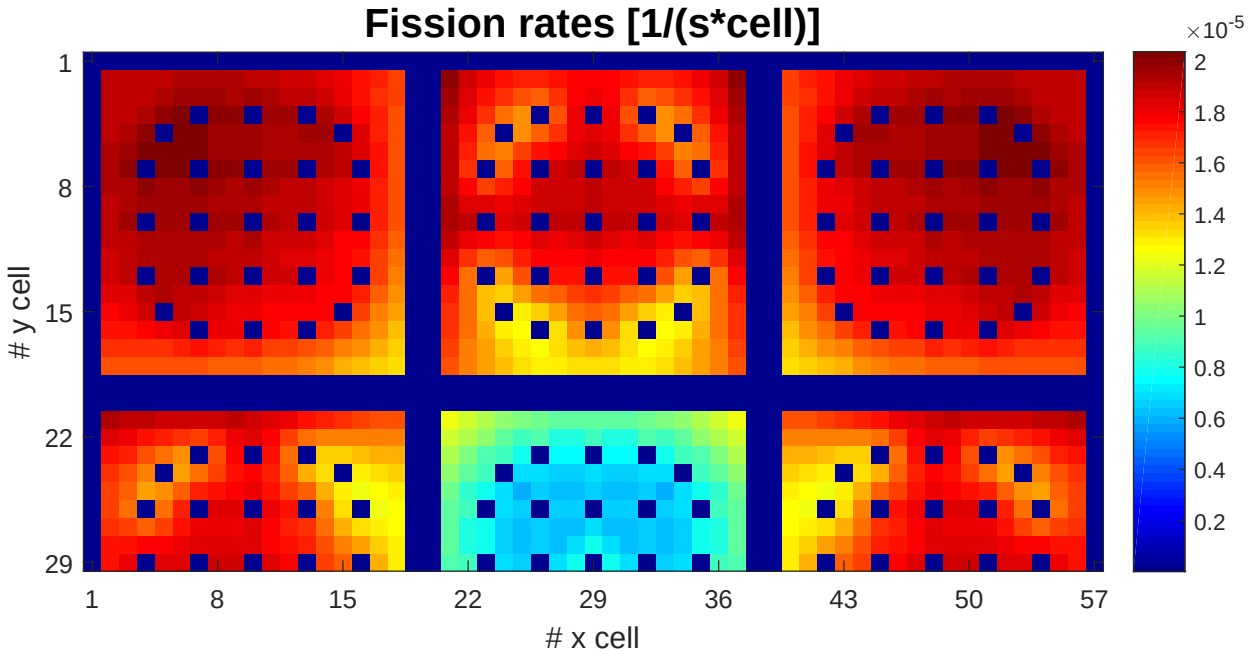

Figure 8: Fission rates for the cluster case described in Sec. 6.

It can be seen that the fission-rate oscillation due to the detector has a quite small amplitude: it peaks at 0.77% in the cell containing the fission chamber and does not go over 0.42% in the two most perturbed fuel cells, to the left and to the right of the previous one. By going towards the boundary, parallel to the oscillation direction, the amplitude decreases up to a value two orders of magnitude lower than the one above. The cells along the perpendicular direction are less affected (about one order of magnitude less) than the previous ones and, clearly, the amplitude of the cells in between assumes intermediate values. These results are nevertheless quite high in comparison to the requirements of an accurate in-core measurement, probably due to the limitations of a 2-D description of the system.

In the case of the rod bundle displacement the measured amplitude is much higher, as it reaches 2.64% in the cells adjacent, along the oscillation direction, to the most external rods (not along the horizontal symmetry axis, though, but along the two successive horizontal rows of control rods). As in the previous case, the effect along the perpendicular direction is about one order of magnitude lower. However, the noise effect appears to be limited to the central assembly: the perturbation in the left and right assemblies peaks at 0.80%, and in the six assemblies above and below the moving rods the maximum amplitude is just 0.30%. This discussion leads to present the main current limitation of the cases analyzed: considering the local temporal fluctuation of fission rates the noise signal does not *propagate* globally and no out-of-phase behavior has been observed.[3] This may be due to the limited size of the system, so that one may be induced to study a larger

[3]The *out-of-phase* second feature characterizes harmonic signals that oscillates with a common frequency but with shifted phases. When present in a system, this feature can be used to localize the origin of the oscillation.

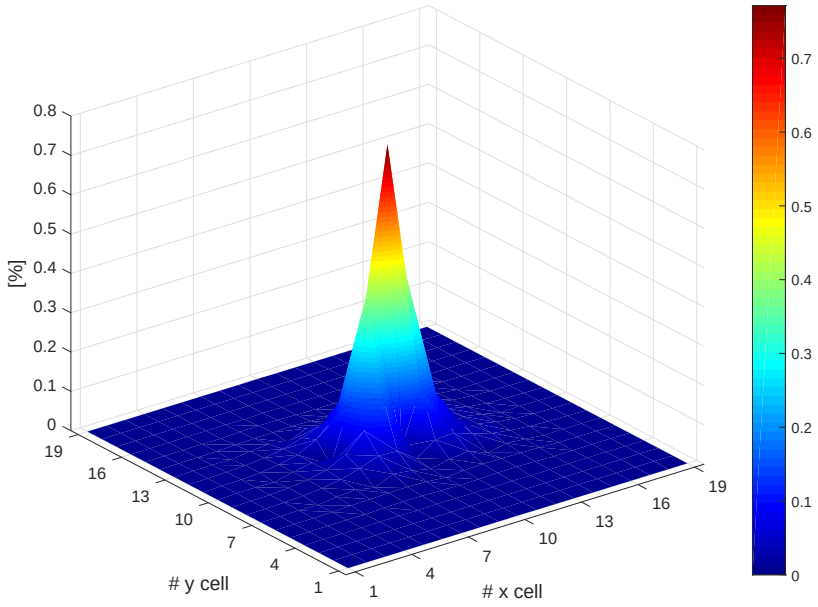

(a)

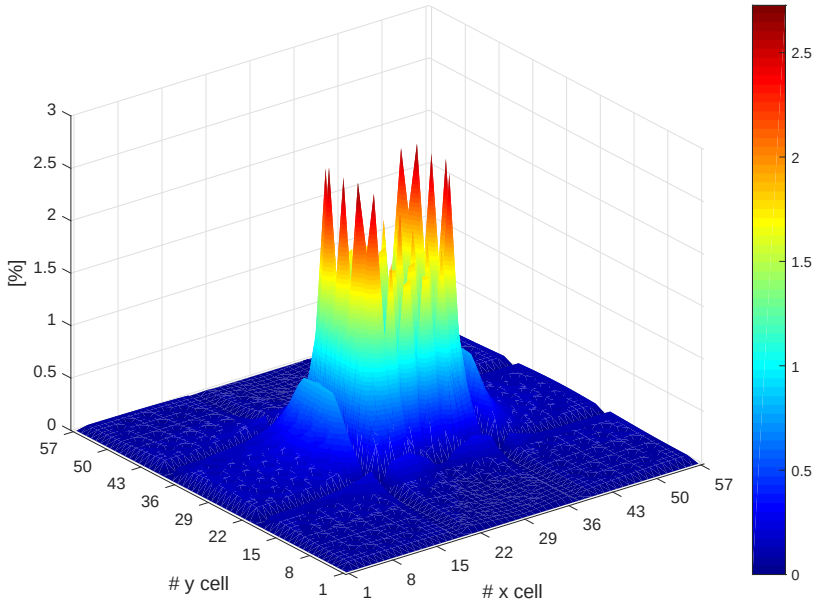

(b)

Figure 9: Fission-rate variation amplitude relative to the period average, plotted over the whole domains for the two case studies (a: detector, b: control rods).

cluster. However, aside for the computational cost that would at least triple, if for the added assemblies the attenuation behaves in the same manner as between the central assembly and its neighbors there would be no less than four orders of magnitude between the most perturbed cell and the one furthest from the center (for a 5×5 cluster): the physical noise would risk to get confused with the numeric one. Future developments should better investigate this aspect. Nevertheless the computed flux fluctuation in the neighboring cells of

rod pins is not negligible and should be considered to correctly simulate thermo-hydraulic behavior of rod bundles.

In any case, the computed oscillation is interesting twofold: on one side, the absence of macroscopic effects on reactivity is consistent with the observed behavior in real systems; on the other side the calculation shows the presence of measurable and important local flux fluctuations that can impact the thermo-mechanical system response.

7. CONCLUSIONS

The noise model presented in this paper simulates periodic oscillations of structural components and analyzes their effects on reactivity and fission rates. The positions over time of the detector and of the control-rod bundle are identified by different geometries, which are linked in the proper order to construct the oscillation period. Following this procedure, noise is studied within the real temporal domain, without the need of Fourier transforming and of the small-perturbation approximation used in the traditional frequency-based approach.

The fission source of delayed neutrons required a specific treatment, leading to express it as a function of the flux values over all the period and, by discretizing the latter in a finite number of sub-intervals, to evaluate the time integral by a quadrature formula suitable for periodic functions.

Each noise iteration is made by a set of outer iterations (one per temporal sub-interval) typical of power methods and updates the newly defined dynamic eigenvalue by means of delayed sources until the convergence of this value and of each fission source over the period. The DP_N synthetic acceleration is employed to achieve a faster convergence of the noise iterations, by accelerating the outer iterations relative to each temporal point.

Looking at our results, the oscillations produce a relevant noise with regard to fission rates: in particular, for the control-rod case the amplitude reaches 2.64% of the period average value. The reactivity is much less affected, as the deviation of the dynamic eigenvalue from the static situation is practically insignificant, at least for nuclear engineering. This is somehow a reassuring result, since practical experience in nominal operating has never shown evident effects on reactivity due to vibrating rods. On the other hand, we have limited our analysis to cases that are not very large: regarding the detector assembly, because a 2-D domain cannot accurately describe an actual configuration, since an object measured in centimeters is inserted in a system of several meters high; as for the rod bundle because, due to the combination of a relatively weak noise source and a relatively small domain, no phase shift has been detected, making it difficult to imagine to apply non-intrusive detection techniques for the cases we have studied.

In conclusion, the temporal noise model shows fluctuations of per-cell fission rates, suggesting the possibility of detecting structure vibrations by analyzing variations of the local flux. In the future, one may be interested in studying larger and even 3-D geometries, which would permit to measure the noise effect on a relevant portion of a reactor and, potentially, on its totality. In particular, a whole oscillating assembly is a promising

candidate as noise source: the hope is to be able to detect some out-of-phase behavior, that would open the doors to frequency analysis.

Finally we note that our preliminary tests show that our technique to deduce *locally* weighted fission spectra, which we think that is more faithful to the physical reality, has an important impact on static reactivities for heterogeneous assembly cases. This incites to pursue further investigations to understand if this model can routinely be used to improve standard (static) calculations.

8. APPENDIX A: Model for neutron leakage

In this appendix we illustrate the leakage model. In order to increase the representativeness of our approach we have in fact used this traditional tool to simulate the impact of the finite reactor size over lattice calculations. The model described in this section is based on Sanchez (2002).

Starting from any heterogeneous domain, in order to have $k_{eff} = 1$ one may think of modifying the streaming term of the transport equation accordingly, either increasing or lowering neutron leakages from the system. This task is simplified by considering a homogeneous medium, equivalent to the initial heterogeneous one, for which a leakage coefficient is computed assuming that it remains valid for the heterogeneous case. This strategy is called "homogeneous leakage approximation", and the assumption is based on is reasonable if the system anisotropy is not too pronounced: for instance, in PWRs there are for sure anisotropic effects due to the vertical disposition of the fuel, but they are traditionally neglected in 2-D models.

First, we want to show how the leakage coefficient appears for an infinite homogeneous and isotropic critical medium. In this case, the transport equation reads

$$(\vec{\Omega} \cdot \nabla + \Sigma_t)\psi = q, \tag{47}$$

where

$$q(\vec{r}, \vec{\Omega}, E) = \int_E dE' \int_{4\pi} d\Omega' \; \Sigma_s(\vec{\Omega}' \cdot \vec{\Omega}, E' \to E)\psi(\vec{r}, \vec{\Omega}', E') + \frac{1}{4\pi}(\mathcal{F}\phi)(\vec{r}, E),$$
$$(\mathcal{F}\phi)(\vec{r}, E) = \sum_j \chi_j(E) \int_E dE' \; (\nu\Sigma_{f,j})(E')\phi(\vec{r}, E'). \tag{48}$$

The flux solution is to be found in the form

$$\psi(\vec{r}, \vec{\Omega}, E) = \psi(\vec{B}, \vec{\Omega}, E)e^{-i_u \vec{B} \cdot \vec{r}}, \tag{49}$$

$\vec{B}$ being the buckling vector. Hence, Eq.(47) translates into

$$\big[\Sigma_t(E) - i_u \vec{B} \cdot \vec{\Omega}\big]\psi(\vec{B}, \vec{\Omega}, E) = q(\vec{B}, \vec{\Omega}, E). \tag{50}$$

Some comments can be made about the relation between $\vec{B}$, ψ and the current $\vec{J}$: the isotropy of the medium implies that the flux and the module of the current depend only on the module of $\vec{B}$ (because they do not vary if $\vec{B}$ and $\vec{\Omega}$ rotate simultaneously). Moreover, it follows from (50) that $\vec{\Omega}$ and $\vec{J}(B, E)$ have the same

direction, since the dependency of the angular flux on $\vec{B}$ is limited to the product $\vec{B}\cdot\vec{\Omega}$ because the medium is invariant under a rotation of axis $\vec{B}$. According to these considerations, by integrating eq. (50) over angles the conservation equation is obtained in the form

$$i_u BJ(B,E) - \Sigma_t(E)\phi(B,E) + Q(B,E) = 0. \tag{51}$$

Defining now a coefficient D as

$$D(B,E) = -\frac{i_u J(B,E)}{B\phi(B,E)}, \tag{52}$$

from (51), the real flux $\phi(\vec{r},E) = \int_{4\pi} d\Omega\psi$ turns out to be solution of the multigroup diffusion equation

$$\left[D(B,E)\nabla^2 - \Sigma_t(E)\right]\phi(\vec{r},E) + Q(\vec{r},E) = 0 \tag{53}$$

having (52) as diffusion coefficient.

Considering now the original heterogeneous problem, we would like to introduce a leakage coefficient defined as D for the homogeneous case. To do that the following factorization for the flux ψ_R is adopted:

$$\psi_R(\vec{r},\vec{\Omega},E) = f(\vec{r})\psi(\vec{r},\vec{\Omega},E), \tag{54}$$

f being the macroscopic flux, result of the material balance over the entire core, and ψ the local one, affected by variations of cross sections on a local scale (fuel cell, assembly or cluster). Therefore, the transport equation can be written as

$$\left[\vec{\Omega}\cdot\left(\nabla + \frac{\nabla f}{f}\right) + \Sigma_t\right]\psi = q \tag{55}$$

which, integrated over angles, reads

$$\left(\nabla + \frac{\nabla f}{f}\right)\cdot\vec{J}(\vec{r},E) + \Sigma_t\phi(\vec{r},E) = Q(\vec{r},E), \tag{56}$$

where only the dependencies of the new terms are shown. At this point, the homogeneous leakage approximation is introduced: first, the macroscopic flux is assumed of the form $e^{-i_u\vec{B}\cdot\vec{r}}$, as in an infinite homogeneous medium, so that $\frac{\nabla f}{f} = -i_u\vec{B}$; then, one supposes that the r.h.s. of this last relation can be expressed by means of (52), that is, using a coefficient independent of the spatial position (hence the name of "homogeneous" leakages) and of the angle. The approximation, reading

$$\frac{\nabla f}{f}\cdot\vec{J} \approx DB^2\phi, \tag{57}$$

can therefore be substituted in (56). This latter is integrated over the chosen "local" spatial domain of volume V_D to give its homogenized version:

$$(-DB^2 - \Sigma_{t,D})\phi_D(E) + Q_D(E) = V_D^{-1}\int_{\delta D} d\vec{S}\cdot\vec{J}(\vec{r},E). \tag{58}$$

The subscript D refers to average volumetric values and $\Sigma_{t,D}$ results from the homogenization made by the flux. Considering that the current is null on a perfectly reflective boundary, Eq. (58) acquires the same form

of (53): it therefore describes the behavior of a homogeneous medium equivalent to the real one. As can be seen, DB^2, that is the product of the leakage coefficient and the critical buckling, modifies the total cross section in order to have a critical system (it can be thought of as an additional absorption cross section).

The procedure to implement this model in our code is iterative, because the homogenized cross sections, needed to evaluate the leakage coefficient, depend on the heterogeneous flux, which in turn depends on the leakage. The required steps can be summarized as follows:

1 update of homogenized cross sections relative to the equivalent homogeneous medium;

2 evaluation of the homogeneous leakage coefficient;

3 evaluation of the critical buckling;

4 introduction of DB^2 into the cross sections (total or scattering);

5 update of the heterogeneous flux.

This cycle has to be repeated until k_{eff} converges to the unit value.

The leakage coefficient and the critical buckling are computed only for the central static configuration, to ensure that the noise actually starts from a critical condition, and are therefore used for all temporal points.

ACKNOWLEDGEMENTS

This work was partially supported by the CORTEX project, which received funding from the Euratom Research and Training Program 2014-2018 under grant agreement No 754316.

References

Adams, M.L., Larsen, E.W., 2002. Fast iterative methods for discrete-ordinates particle transport calculations. Progress in Nuclear Energy 40, 3–159. doi:https://doi.org/10.1016/S0149-1970(01)00023-3.

Brun, E., Damian, F., Diop, C., Dumonteil, E., Hugot, F., Jouanne, C., Lee, Y., Malvagi, F., Mazzolo, A., Petit, O., Trama, J., Visonneau, T., Zoia, A., 2015. Tripoli-4®, cea, edf and areva reference monte carlo code. Annals of Nuclear Energy 82, 151–160. doi:https://doi.org/10.1016/j.anucene.2014.07.053.

Dugan, K., Zmijarevic, I., , Sanchez, R., 2016. Cross-section homogenization for reactivity-induced transient calculations. Journal of Computational and Theoretical Transport 45, 425–441. doi:10.1080/23324309.2016.1188116.

Dulla, S., Ravetto, P., Rostagno, M.M., 2004. Neutron kinetics of fluid-fuel systems by the quasi-static method. Annals of Nuclear Energy 31, 1709–1733. doi:https://doi.org/10.1016/j.anucene.2004.05.004.

Hfaiedh, N., Santamarina, A., 2005. Determination of the optimized shem mesh for neutron transport calculations. Proc. Int. Mtg. Mathematics and Computations (M&C) .

Hildebrand, F.B., 1954. Introduction to Numerical Analysis. Dover Publications.

Keepin, G.R., 1965. Physics of nuclear kinetics. Addison-Wesley series in nuclear science and engineering, Addison-Wesley Pub. Co.

Kochunas, B.C., Larsen, E.W., Xu, Y., 2017. Space-dependent wielandt shifts for multigroup diffusion eigenvalue problems. Nuclear Science and Engineering 188, 140–159. doi:10.1080/00295639.2017.1350001.

Mao, L., Zmijarevic, I., Routsonis, K., 2019. Application of the sph method to account for the angular dependence of multigroup resonant cross sections in thermal reactor calculations. Annals of Nuclear Energy 124, 98–118. doi:https://doi.org/10.1016/j.anucene.2018.09.031.

Masiello, E., Sanchez, R., Zmijarevic, I., 2009. New numerical solution with the method of short characteristics for 2-d heterogeneous cartesian cells in the apollo2 code: Numerical analysis and tests. Nuclear Science and Engineering 161, 257–278. doi:10.13182/NSE161-257.

Mosca, P., Mounier, C., Bellier, P., Zmijarevic, I., 2013. Improvements in transport calculations by the energy dependent fission spectra and subgroup method for mutual self-shielding. Nuclear Science and Engineering 175, 266–282. doi:10.13182/NSE12-63.

Pázsit, I., Demazière, C., 2010. Noise Techniques in Nuclear Systems. Springer US, Boston, MA. pp. 1629–1737. doi:10.1007/978-0-387-98149-9_14.

Ravetto, P., 1997. Reactivity oscillations in a point reactor. Annals of Nuclear Energy 24, 303–314. doi:https://doi.org/10.1016/S0306-4549(96)00066-7.

Rouchon, A., 2016. Analyse et développement d'outils numériques déterministes et stochastiques résolvant les équations du bruit neutronique et applications aux réacteurs thermiques et rapides. Theses. Université Paris-Saclay. URL: https://tel.archives-ouvertes.fr/tel-01381245.

Sanchez, R., 2002. Calcul des fuites. Internal Technical Report DMT CEA, Commissariat à l'Energie Atomique et aux Energies Alternatives .

Sanchez, R., 2015. Some comments in neutron noise theory. Annals of Nuclear Energy 86, 88–98. doi:https://doi.org/10.1016/j.anucene.2015.04.003.

Sanchez, R., Mao, L., Santandrea, S., 2002. Treatment of boundary conditions in trajectory-based deterministic transport methods. Nuclear Science and Engineering 140, 23–50. doi:10.13182/NSE140-23.

Santamarina, A., Bernard, D., Blaise, P., Coste, M., Courcelle, A., Huynh, T., Jouanne, C., Leconte, P., Litaize, O., Mengelle, S., Noguère, G., Ruggiéri, J.M., Sérot, O., Tommasi, J., Vaglio, C., Vidal, J.F., 2009. The jeff-3. 1. 1 nuclear data library. Technical Report JEFF Report 6807 .

Santandrea, S., 2007. An integral multidomain dpn operator as acceleration tool for the method of characteristics in unstructured meshes. Nuclear Science and Engineering 155, 223–235. doi:10.13182/NSE155-223.

Santandrea, S., Sciannandrone, D., Sanchez, R., Mao, L., Graziano, L., 2017. A neutron transport characteristics method for 3d axially extruded geometries coupled with a fine group self-shielding environment. Nuclear Science and Engineering 186, 239–276. doi:10.1080/00295639.2016.1273634.

Stankovski, Z., 2011. La java de silène, a graphical user interface for 3d pre & post processing: State-of-the art and new developments. Proc. Int. Mtg. Mathematics and Computations (M&C) .

Viebach, M., Bernt, N., Lange, C., Hennig, D., Hurtado, A., 2018. On the influence of dynamical fuel assembly deflections on the neutron noise level. Progress in Nuclear Energy 104, 32–46. doi:https://doi.org/10.1016/j.pnucene.2017.08.010.

Weinberg, A.M., Schweinler, H.C., 1948. Theory of oscillating absorber in a chain reactor. Physical Review 74, 851–863. doi:10.1103/PhysRev.74.851.

Time interval	Fission integral
1	0.73302
2	1.12530
3	1.34575
4	1.12978
5	0.73304
6	1.12398
7	1.34570
8	1.12855

Table 4: Fission integrals over time.

# static	Eigenvalue
1	0.73572
2	0.73839
3	0.73918
4	0.73839
5	0.73572
6	0.73839
7	0.73918
8	0.73839

Table 5: Static eigenvalues.

Table 6: Eigenvalue results

Moving component		Detector	Rod bundle
Static eigenvalues	1	1.000006	1.000003
	2	1.000001	0.999970
	3	0.999998	0.999876
	4	1.000001	0.999970
	5	1.000008	1.000003
	6	1.000001	0.999971
	7	0.999998	0.999878
	8	1.000001	0.999971
Dynamic eigenvalue $(f = 1\ Hz)$		1.000004	0.999946